行政院國家科學委員會補助專題研究計畫 ■成果報告 □期中進度報告

（計畫名稱）延遲性耦合震盪系統

Coupled Oscillators with Delays

計畫類別：■個別型計畫　□整合型計畫

計畫編號：NSC 98-2115-M-009-012-MY3

執行期間：98 年 08 月 01 日起至民國 101 年 07 月 31 日

執行機構及系所：交通大學應用數學系

計畫主持人：石至文

共同主持人：

計畫參與人員：廖康伶 蔡澤弘 陳冠維

成果報告類型(依經費核定清單規定繳交)：□精簡報告 ■完整報告

本計畫除繳交成果報告外，另須繳交以下出國心得報告：

□赴國外出差或研習心得報告

□赴大陸地區出差或研習心得報告

■出席國際學術會議心得報告

□國際合作研究計畫國外研究報告

處理方式：除列管計畫及下列情形者外，得立即公開查詢

□涉及專利或其他智慧財產權，□一年■二年後可公開查詢

中　華　民　國　　年　　月　　日

中文摘要：

本計劃探討具延遲性之耦合震盪系統之動態行為。我們考慮與感興趣的系統包括一些生物系統與神經細胞模型。目前進行的有一斑馬魚骨節生成的模型、FitzHugh-Nagumo model on neurons, Morris-Lecar model on neurons及一些artificial neural models。我們探討的耦合系統行為包括同步化(synchronization)、同步震盪（synchronous oscillation）、反相同步化(anti-phase synchronization)等。系統在不同參數及不同時間延遲下可能收斂到同步常態解、同步周期解、非同步周期解等。我們已發表三篇論文，另有二篇論文投稿中，一篇論文準備投稿中。

有關 neural networks，去年發表一篇論文 Global synchronization and asymptotic phases for a ring of identical cells with delayed coupling 於 SIAM J. Mathematical Analysis。在這工作裡，我們討論系統的同步化及可能的最終同步行為，包括對稱的單平衡點、多平衡點、同步周期解、非同步周期解。我們分析這些行為與系統的大小、重要參數、遲滯項的大小之關連。我們也探討由遲滯項的影響而產生的震盪及同步化的失去。依我們所建立的分析方法，我們回答了文獻中的兩個猜想。

有關斑馬魚骨節生成之 segmentation clock genes 模型之數學研究已發表兩篇論文:

K.-L. Liao, C.-W. Shih* and J.-P. Tseng, 2012, “Synchronized oscillations in a Mathematical model of segmentation in zebrafish”, Nonlinearity 25, 869–904.

K.-L. Liao, C.-W. Shih*, 2012, “A lattice model on somitogenesis of zebrafish”, Discrete and Continuous Dynamical Systems –Series B, 17 (8).

在前一篇文章裡，我們考慮的是兩個coupled cells, 共八個delay equations 的系統，主要探討的是在什麼參數條件下，系統能產生周期為30 分鐘之同步周期解，此為對應 zebrafish 骨節每節生成的時間，及推導oscillation-arrested 的條件，此對應生成調控之一個階段，進而瞭解參數範圍所對應的動態行為；其中周期解的存在是用delay Hopf bifurcation theory 做的，計算相當繁複。此外，我們也做了不少數值模擬，一方面驗證理論，一方面延伸結論。在後一篇文章裡，我們考慮的是一個N網格模型，在理論基礎之下，設計出參數隨時間及空間的變化，方程式解的行為對應骨節生成中主要的基因表現動態。我們所建構的方法可以用來處理其它的 gene regulatory models，並進一步探討生物時鐘、生物韻律的數學模型。這部份的工作正在進行中，並納入下一期計畫的內容中。

有關 neuron model，我們建構一個 general framework，改良先前的 iteration scheme，使得我們的方法可以應用在 coupled FitzHugh-Nagumo neurons 及 Morris-Lecar neuron neuron 之 synchronization，under gap junction (linear, diffusive) coupling 或(nonlinear) synaptic coupling with transmission delay，已完成一篇論文投稿。

這幾年，我們發展了一個方法(想法)，研究 nonlinear systems 及 coupled nonlinear systems, with delay or without delay 的 asymptotic behaviors，包含 global convergence to single equilibrium, existence of multiple equilibrium points，multistability, convergent dynamics with multiple equilibria (or almost periodic orbits), synchronization, synchronous oscillations, anti-phase oscillations 等，後二者配合運用 delay Hopf bifurcation theory。過去，一般而言，研究 global dynamics 多依賴 Lyapunov function technique；其次，某些系統可運用 monotone dynamics theory。但對複雜的非線性系統或延遲系統(including time-dependent delay), 這兩種方法頗不可行。我們的方法，稱 sequential upper-lower-dynamics technique，目前已運用到一些系統，可以解決一些以前的工具沒辦法解決的問題。過去文獻所使用的數學工具相當有限，其研究 local dynamics 或 bifurcation of spatio-temporal patterns，多依賴 linearization 及 equivariant bifurcation theory。這些工具很不容易做到 combined effect of parameters and delays upon the dynamics 結果。Delay 的大小影響 dynamics，但對非線性延遲系統 with multiple delays，如果系統整個 asymptotic behaviors 不是那麼單純，很少有數學結果明確說多大多小的 delay，配合什麼樣的參數，是如何改變 dynamics。我們引入了新的方法，也得到新的結果；我們相信這對非線性動力學中 coupled nonlinear systems with delays 的研究提供了新的思維；而這些想法也讓我們可以處理其他生物數學的 models，包含一些 integral-differential equations，multiple- component systems with multiple delays or distribution delays。

關鍵詞: 收斂動態、震盪凍結、遲滯方程、同步化、同步周期解、多穩定性、神經網路、分歧性、基因調控、體節生成

英文摘要:

We are interested in the dynamics for systems composed of subsystems with delayed connection. The subsystems themselves can have time delay of magnitude different from the connection delay. The systems we study include some gene regulatory networks such as kinetic models for segmentation clock gene of zebrafish, and neuronal models.

For neural network models, we published a paper “Global synchronization and asymptotic phases for a ring of identical cells with delayed coupling” in SIAM J. Mathematical Analysis. In this work, we consider a neural network which consists of a ring of identical neurons coupled with their nearest neighbors. Self-feedback delay and transmission delay are also taken into account in the network. We investigate synchronization and various synchronous phases for the system. The possible asymptotical dynamics include convergence to single equilibrium or multiple equilibria, synchronous oscillations, and asynchronous oscillations in the form of standing wave. We elucidate the effects from the scale of network, self-decay, self-feedback strength, coupling strength and delay magnitude upon synchrony, convergent dynamics and oscillation of the network. The disparity between the contents of synchrony induced by distinct factors is investigated. Two different types of multistable dynamics are distinguished. Moreover, oscillation and desynchronization induced by delays are addressed. We then answer two conjectures in the literature.

For the kinetic models for segmentation clock gene of zebrafish, we have published two papers [K.-L. Liao, C.-W. Shih* and J.-P. Tseng, 2012, “Synchronized oscillations in a Mathematical model of segmentation in zebrafish”, Nonlinearity 25, 869–904], [K.-L. Liao, C.-W. Shih*, 2012, “A lattice model on somitogenesis of zebrafish”, Discrete and Continuous Dynamical Systems –Series B, 17 (8)]. Somitogenesis is a process for the development of somites which are transient, segmental structures that lie along the anterior-posterior axis of vertebrate embryos. The pattern of somites is traced out by the segmentation clock genes” which undergo synchronous oscillation over adjacent cells. In the first work, we analyze the dynamics for a model on zebrafish segmentation clock-genes which are subject to direct autorepression by their own products under time delay, and cell-to-cell interaction through Delta-Notch signaling. For this system of delayed equations, an ingenious iteration approach is employed to derive the global synchronization and global convergence to the unique synchronous equilibrium.

On the other hand, by applying the delay Hopf bifurcation theory and the method of normal form, we derive the criteria for the existence of stable synchronous oscillations. Our analysis provides the basic range of parameters and delay magnitudes for stable synchronous, asynchronous oscillation, and oscillation-arrested dynamics. Based on the derived criteria, further numerical findings on the dynamics which are linked to the biological phenomena are explored for the considered system. In the second work, we consider lattice systems which describe the kinetics of the chief segmentation clock genes in zebrafish under negative feedback regulation with delay through interaction with the Delta-Notch signaling among neighboring cells. We first derive the analytical theories for the oscillation-arrested and synchronous oscillation in an autonomous lattice model. Based on the parameter regimes in the theories, we design suitable gradients of degradation rates and delays in a non-autonomous lattice model. Such a lattice system can generate synchronous oscillations, oscillatory traveling waves, oscillation slowing down, oscillation-arrested, and high-low expression levels. We further distinguish between different gradient structures which lead to normal and abnormal segmentations respectively and connect these structures to the dynamical regimes in the cell-cell model.

Keywords: Convergent dynamics, Oscillation-arrested, Delayed equation, Synchronization, Synchronous oscillation, Multistability, Neural network, Bifurcation, Segmentation clock gene

報告內容:

1. 研究目的、文獻探討

Asymptotic behaviors and collective dynamics for nonlinear systems and coupled nonlinear systems have been major research subjects in dynamical systems of mathematics discipline and nonlinear dynamics of physics discipline. Nevertheless, mathematical methodologies in concluding global dynamics and asymptotic behaviors for nonlinear systems and delay equations are quite limited. The classical approaches are Lyapunov function method and monotone dynamics theory. However, for complex nonlinear systems, construction of Lyapunov function or partial order in phase space is often infeasible. In fact, one sees that Lyapunov functions are expressed by basic functions, whereas the solutions of differential equations are functions in general sense. The insufficiencies of Lyapunov method (or Krasovskii theorem) have been revealed in several works; for example, Slotine from MIT introduced the "Contraction analysis" [E. Slotine et al.,1998, *On contraction analysis for nonlinear systems*, Automatica 34 (6)]。From there, a series of research works has been reported. However, this approach was not formulated under mathematical rigorousness: the displacement equation or variational equation is not precisely defined from the considered equations. If we extend the interpretation under precise mathematical sense, then that consideration is too restricted, as using the eigenvalues of certain corresponding linear systems to obtain the dynamics of the original nonlinear systems leads to local dynamics or merely partial behaviors. On the other hand, for equations with multiple delays, analyzing the linearized equations is another complex task, as seen in several works in the literature (e.g. the ones by S. A. Campbell).

Time delays exist in circuit systems, mechanical systems, physical systems, biological systems, and traffic flows. Taking delay into account in differential equations raises the phase space to infinite dimension. While regarded as a functional differential equation, delay equation admits certain technical difficulty and its fundamental theory, especially for the case of state-dependent delay, was just developed recently. The role that time delay plays in mathematical modeling in application fields has never been overemphasized. For example, time lags, accounting synthesis and trafficking of macromolecules in cells, are required to generate oscillation in gene regulation models, as illustrated in [J. Lewis, 2003, Autoinhibition with transcriptional delay: a simple mechanism for the zebrafish somitogenesis oscillator, Curr. Biol.]. Nevertheless, the theory driven by the application of delay-modeling requires further mathematical ideas and developments, especially for systems with multiple delays and distribution delay.

Synchronous behavior is ubiquitous in nature, for example, simultaneous

flashing of fireflies, crickets chirping in unison, synchronous activity of pacemaker cells in the heart, and synchronized bursts of pancreatic beta-cells. There is a large literature on synchronization in physics and applied mathematics. Concerning synchronization of coupled neurons, say models of Hodgkin-Huxley, Morris-Lecar, FitzHugh-Nagumo, Hindmarsh-Rose, there are some mathematical results if the neurons are under gap junction (linear, diffusive) coupling, but there does not exit analytical result if the neurons are under synaptic coupling with delayed transmission (most neurons are actually coupled via chemical synapses), as commented in [E. Steur et al., 2009, Semi- passivity and synchronization of diffusively coupled neuronal oscillators, Physica D, 238] .

Mathematical models for gene regulatory networks usually consist of multiple components if there are several genes involved and their mRNA and proteins are considered. For example, the basic mathematical cell-cell models on segmentation clock gene of zebrafish are systems with at least eight components and four delays which are incurred in the transcription and translation processes. The basic dynamical phases for such models are synchronous oscillation and oscillation-arrested. Mathematical analysis had been absent in investigating those mathematical models. In fact, it was commented in [R. E. Baker, S. Schnell, 2010, *How can mathematics help us explore vertebrate segmentation* ? HFSP Journal, 3:1] that the majority of the models are incredibly difficult to analyze mathematically. Almost all the existing results are obtained through numerical simulations. Yet the studies based on numerical computations in the literature contain certain shortcoming, as remarked in [Uriu, Morishita, Iwasa, 2009, Synchronized oscillation of the segmentation clock gene in vertebrate development, J. Math. Biol.]; for example, convergence to the numerically observed periodic orbit is slow, since the dynamical property of such orbit is unknown. Moreover, the basin of attraction for the oscillation is very small, and hence the oscillation is difficult to observe in phase space of high dimension.

Mathematical models on biology typically involve many parameters (one or two dozens). It is a highly nontrivial task to understand the dynamics corresponding to various parameter values and their various combinations through numerical computations. Combining analysis and numerical computation is the best approach in investigating mathematical models. However, developing effective mathematical approaches to treat complex nonlinear systems with multiple components and/or multiple delays is itself a challenge for applied mathematicians.

2. 研究方法:

We have developed a mathematical approach (idea) to investigate the asymptotic behaviors of nonlinear systems and coupled nonlinear systems, with delay or without delay, including global convergence to single equilibrium, existence of multiple equilibrium points, multistability, convergent dynamics with multiple equilibria (or almost periodic orbits), synchronization, synchronous oscillations, and anti-phase oscillations. For the latter two on oscillation, delay Hopf bifurcation theory has also been employed. Our methodology, named "sequential contracting", has been applied to a number of systems and resolved some unsolved problems. Designs of pertinent upper and lower bounds which lead to the targeted asymptotic dynamics is the first key step in applying sequential contracting. The methodology allows us to establish global synchronization and multistability under delay-independent or delay-dependent criteria through different designs of upper and lower dynamics. For network systems, we can also derive scale-dependent criteria (scale is the network size) for synchronization. Under our formulation, these nonlinear problems are reduced to linear problems in a form of Gauss-Seidel iterations. Delays modify dynamics, but analytic finding depicting how delays and what magnitudes of delays change the dynamics is rare, especially for systems with nontrivial asymptotic phases (not just an equilibrium). Our approach provides new thoughts in treating multiple-component systems with multiple delays or distribution delays, which leads to developing analytic studies on nonlinear mathematical models on biology.

3. 結果與討論

[K.-L. Liao, C.-W. Shih*, 2012, "A lattice model on somitogenesis of zebrafish", Discrete and Continuous Dynamical Systems –Series B, 17 (8)].

DISCRETE AND CONTINUOUS
DYNAMICAL SYSTEMS SERIES B
Volume **17**, Number **8**, November **2012**

doi:10.3934/dcdsb.2012.17.2789

pp. **2789–2814**

A LATTICE MODEL ON SOMITOGENESIS OF ZEBRAFISH

Kang-Ling Liao and Chih-Wen Shih*

Department of Applied Mathematics
National Chiao Tung University
Hsinchu 300, Taiwan

Abstract. Somitogenesis is the process of the development of somites which are segmental structure in vertebrate embryos. This process depends on the expression of segmentation clock genes. In this investigation, we consider lattice systems which describe the kinetics of the chief segmentation clock genes in zebrafish under negative feedback regulation with delay through interaction with the Delta-Notch signaling among neighboring cells. We first derive the analytical theories for the oscillation-arrested and synchronous oscillation in an autonomous lattice model. Based on the parameter regimes in the theories, we design suitable gradients of degradation rates and delays in a non-autonomous lattice model. Such a lattice system can generate synchronous oscillations, oscillatory traveling waves, oscillation slowing down, oscillation-arrested, and high-low expression levels. We further distinguish between different gradient structures which lead to normal and abnormal segmentations respectively and connect these structures to the dynamical regimes in the cell-cell model.

1. **Introduction.** In vertebrate embryos, somites are segmental structure which arises one by one from the presomitic mesoderm (PSM) and lies along the anterior-posterior (AP) axis. Under further development, somites develop into vertebrate, rib, and tail. The whole process of the development of somites, which involves gene regulation in both space and time, is called *somitogenesis*. During the process, the embryo can be divided into five regions: head, other tissues, determined region (DR), traveling wave region (TWR), and the tail bud (TB), successively.

For zebrafish, somite segmentation depends on the expression of clock genes *her*1 and *her*7, with neighboring cells interacted through Delta-Notch signaling [15, 16, 21, 23, 25]. It has been observed in biological experiments that gene expression shows synchronous oscillation in the tail bud, and traveling wave pattern arises from the posterior end and moves toward the anterior end of the TWR. The oscillations then slow down, and finally arrest and cells form into somites. In addition, the oscillation period of clock genes in the tail bud of zebrafish is about 30 minutes which match the time interval for somite formation [13, 14]. This indicates that the period of the synchronously oscillating gene expression plays an important role in controlling when the somites form. On the other hand, the slowing down of oscillation is controlled by other proteins. Biologists have discovered that the signaling molecule *fibroblast growth factor* (FGF) regulates differentiation of the PSM cells [10, 17, 32]. Moreover, FGF is only transcribed at the posterior tip of

2000 *Mathematics Subject Classification.* Primary: 92B25, 37N25, 34K18, 34K13.
Key words and phrases. Somitogenesis, lattice model, oscillation-arrested, synchronous oscillation, traveling wave.
* corresponding author.

the embryo and progresses from the posterior to the anterior of the PSM with gradient. In addition, there exists a threshold such that if the FGF is smaller than this threshold, then cells start to differentiate into somites.

Modeling of the "clock and wavefront" for simitogenesis dates back to Cooke and Zeeman in 1976 [7]; therein, an idea of cyclic motion within the PSM cells along with cell fate determination was advocated. Since then substantial investigations through experiment or modeling have been reported. Based on some experimental evidences [8, 9, 12, 14, 24], Baker et al. [4] proposed a "clock and wavefront" PDE model to investigate the pattern formation mechanism, which depends on the somite factor and the gradient of FGF8 expression. In 2003, Lewis [18] proposed a system of delayed differential equations (DDE) which model the negative feedback regulation and intercellular interaction via Delta-Notch signaling into segmentation clock genes kinetics to generate synchronously oscillatory expression. However, his original model can not produce oscillation slowing down and traveling wave pattern. On the other hand, Cinquin [6] proposed a 13-component multicellular DDE model for zebrafish somitogenesis, that involves heterodimerization of clock proteins, Her1 and Her7, with controlling protein Her13.2 [17, 29]. The system was used to model the posterior-anterior slowing of oscillation rate, which leads to formation of clock-wave. Recently, Uriu et al. [30, 31] proposed an ODE model which includes an intermediate process of the gene expression (transport of Her protein from cytoplasm to nucleus) to replace time delay to generate synchronous oscillations and traveling waves. Campanelli and Gedeon [5] investigated the control mechanisms in the formation of gene expression wave. Multiple transcription binding sites and differential decay rates for the monomers and dimers of the clock protein were considered in generating the waveforms to match experimental observations.

From the observed phenomena, synchronous oscillation, traveling wave pattern, oscillation slowing down, and oscillation-arrested are necessary dynamics for normal segmentation. In addition, FGF or Her13.2 is an important factor to control the oscillation slowing down. Mutations in the Notch cell-cell signaling pathway and the abnormal traveling wave pattern disrupt synchronization, somite formation, and lead to defective somite boundary and irregular segmented body axis [16, 18]. Indeed, a number of parts of these phenomena require further analysis to elucidate the whole mechanism for the somitogenesis.

The studies on segmentation clock and the involved internal machinery of the individual cell through mathematical modeling were largely based on numerical simulations, due to the complexity of gene networks. Recently, for Lewis's two-cell model, analytical theories on synchronous oscillations and oscillation-arrested have been established through delay Hopf bifurcation theory and the sequential-contracting technique respectively, in [19]. The work in [19] sheds a light on the investigation of complex gene networks represented by coupled-cell systems. In this paper, we consider the homodimer model which takes *her* gene as either *her*1 or *her*7, and the neighboring cells are interacted through Delta-Notch signaling with delay. We shall extend the theories on synchronous oscillations in the tail bud and oscillation-arrested in the determined region to a lattice model for coupled n cells. Moreover, we show that the oscillation-arrested with high and low expression levels arises for non-identical cells with large degradation rates. Based on the collective behaviors of the multi-cellular model, we shall further modify Lewis's model to a non-autonomous lattice system to generate traveling waves for the segmentation gene expression in zebrafish. We design a suitable anterior-posterior gradient of

degradation rates and delays in the lattice model according to the parameter regimes for the corresponding collective dynamics. The cyclic gene expression in this lattice system then exhibits a pattern of traveling wave. We distinguish between different gradient structures which lead to normal and abnormal segmentations respectively and connect these structures to the dynamical regimes in the autonomous model. It is observed that if the differential degradation rates are not posited properly, then the peaks of oscillation will move in incorrect direction or collide and lead to abnormal segmentation, where the size, forming period, and the number of somites are irregular.

The dynamics for the considered spatiotemporal pattern presented in the form of oscillatory traveling wave are rather intricate, as the synchrony among cells is lost, yet certain coherent rhythm remains. Traveling wave formation for the clock gene expression of zebrafish has also been investigated via an ODE model in [30], where the gradient for the reaction parameters was formulated according to numerical studies on the model. The motivation for this investigation is to illustrate that such a traveling wave also exists in delay model. Moreover, in order to elucidate the somitogenesis through mathematical modeling, on the basis of both analytic theories and numerical simulations, we attempt to link the clock-wave patterns to the collective dynamics of the coupled system and learn the underlying mechanism behind the parameter gradients. In addition, it is appealing to map the factors for normal and abnormal segmentations in the considered model to the cell-cell dynamics.

The above-mentioned models of clock gene expression and their interaction with signaling genes are rather difficult to analyze mathematically. As commented in [3], by forgetting about the internal machinery of the segmentation clock in each cell, researchers have turned to employ the notion of phase function to explore the collected dynamics of the coupled oscillators, where an oscillator represents an oscillatory gene in each cell or a group of synchronous cells [22]. Let us mention other related works. A PDE model which describes the movement of cells via cell-cell adhesion mechanism to investigate pattern formation for the aggregation behavior of cell population was reported in [1]. By including an explicit equation for adhesive cell population to the chemical signaling model in [4], the experimentally observed pattern of cellular aggregate in forming somites was reproduced in [2]. On the other hand, periodic traveling wave, as a non-uniform oscillatory spatiotemporal pattern, occurs in cyclic populations and other ecologically relevant scenarios modeled by oscillatory reaction-diffusion equations [26].

The presentation is arranged as follows. In section 2, we extend the analytic theories for oscillation-arrested and synchronous oscillation for segmentation gene to n-cell system and the asynchronous oscillation for the system of two non-identical cells. Then by using the information of these collective behaviors, in section 3, we construct a non-autonomous lattice model with suitable gradients of degradation rates and delays. Through numerical simulations, we illustrate propagation of oscillatory waves corresponding to normal and abnormal segmentations respectively, and discuss the associated gradient structures. The presentation ends with a conclusion.

2. **Autonomous lattice system.**

In this section, we establish analytical theories for the n-cell kinetic model of clock gene expressions in the cells of zebrafish embryo. Oscillation-arrested for the cells at the DR, asynchronous oscillations at the TWR, and synchronous oscillation at the TB shall be discussed. These theories are

extensions from the investigation of the Lewis's two-cell model in [19]. The results in this section provide a basis for setting up the gradient structure of the activation parameters and delay magnitudes in a non-autonomous system which exhibits traveling wave of gene expression, presented in section 3. We arrange the theories on oscillation-arrested and oscillations in subsections 2.1 and 2.2, respectively. Based on these analytical theories, we summarize the collective behavior of the considered coupled system in subsection 2.3.

We assume that there are n cells located along the AP axis and each cell is identified by index i, $i = 1, \cdots, n$, in succession along the axis. The neighboring cells are interacted through the Delta-Notch signaling. Let $x_{1(i)}, x_{2(i)}, x_{3(i)}, x_{4(i)}$ denote the concentrations of *her* mRNA, Her protein, *delta* mRNA, and Delta protein in cell i, respectively. We consider the following kinetic equations:

$$\begin{cases} \dot{x}_{1(i)}(t) &= g_H(x_{2(i)}(t-\tau_{1(i)}),\ \tilde{x}_{4(i)}(t-\tau_{1(i)})) - d_{1(i)}x_{1(i)}(t) \\ \dot{x}_{2(i)}(t) &= a_2 x_{1(i)}(t-\tau_{2(i)}) - d_{2(i)}x_{2(i)}(t) \\ \dot{x}_{3(i)}(t) &= g_D(x_{2(i)}(t-\tau_{3(i)})) - d_{3(i)}x_{3(i)}(t) \\ \dot{x}_{4(i)}(t) &= a_4 x_{3(i)}(t-\tau_{4(i)}) - d_{4(i)}x_{4(i)}(t), \end{cases} \tag{2.1}$$

where $1 \le i \le n$, $\tilde{x}_{4(i)} = [x_{4(i-1)} + x_{4(i+1)}]/2$, for $i = 2, \cdots, n-1$ and $\tilde{x}_{4(1)} = x_{4(2)}$, $\tilde{x}_{4(n)} = x_{4(n-1)}$. Herein, a_2 (resp., a_4) is the protein synthesis rate per mRNA molecule for *her* (resp., *delta*) gene; $d_{1(i)}, d_{2(i)}, d_{3(i)}, d_{4(i)}$ are the degradation (decay) rates for *her* mRNA, Her protein, *delta* mRNA, and Delta protein for cell i, respectively; $\tau_{1(i)}, \tau_{2(i)}, \tau_{3(i)}, \tau_{4(i)}$ are positive numbers which represent the time delays in the processes of *her* gene transcription, *her* gene translation, *delta* gene transcription, and *delta* gene translation and delivery to cell membrane for cell i, respectively. Functions g_H and g_D relate the transcription initiation rates to *her* mRNA and *delta* mRNA concentrations respectively; they are represented by

$$g_H(u,v) := k_H \frac{1 + \frac{v}{P_{D_0}}}{1 + \frac{v}{P_{D_0}} + \frac{u^2}{P_0^2}}, \tag{2.2}$$

$$g_D(u) := \frac{k_D}{1 + \frac{u^2}{P_0^2}}, \tag{2.3}$$

for $u, v \ge 0$; k_H (resp., k_D) is the maximal synthesis rate of *her* (resp., *delta*) mRNA; P_0 (resp., P_{D_0}) is the critical number of molecules of Her (resp., Delta) protein per cell for inhibition of transcription (resp., activation of Notch). Note that the rate of $x_{1(i)}$, the *her* mRNA for the cell located at i, $1 < i < n$, is promoted by the amount $[x_{4(i-1)} + x_{4(i+1)}]/2$ which is the average of the Delta proteins of the neighboring cells at $(i-1)$ and $(i+1)$. For the cell at $i = 1$ or $i = n$, there is only one neighboring cell. Both *her* mRNA and *delta* mRNA are suppressed by their own Her proteins, as expressed in the definitions of g_H and g_D.

We call system (2.1) the one for "n identical cells" if $\tau_{j(i)} = \tau_{j(1)}$, for all $i = 2, 3, \cdots, n$ and $j = 1, 2, 3, 4$, and

$$d_{j(i)} = d_{j(1)}, \text{ for all } i = 2, 3, \cdots, n, \text{ and } j = 1, 2, 3, 4; \tag{2.4}$$

i.e., (2.1) becomes

$$\begin{cases} \dot{x}_{1(i)}(t) &= g_H(x_{2(i)}(t-\tau_1),\ \tilde{x}_{4(i)}(t-\tau_1)) - d_1 x_{1(i)}(t) \\ \dot{x}_{2(i)}(t) &= a_2 x_{1(i)}(t-\tau_2) - d_2 x_{2(i)}(t) \\ \dot{x}_{3(i)}(t) &= g_D(x_{2(i)}(t-\tau_3)) - d_3 x_{3(i)}(t) \\ \dot{x}_{4(i)}(t) &= a_4 x_{3(i)}(t-\tau_4) - d_4 x_{4(i)}(t), \end{cases} \tag{2.5}$$

for $1 \le i \le n$, where $d_j = d_{j(1)}$ and $\tau_j = \tau_{j(1)}$, $j = 1, 2, 3, 4$. Herein, we call (2.1) the system for "n non-identical cells", if (2.4) does not hold. We interpret that cells having different degradation rates is a consequence of gradient FGF.

We consider the evolution $\Psi(t, \phi)$ of (2.1) from initial condition $\phi = (\phi_1, \cdots, \phi_{4n}) \in \mathcal{C}([-\tau_M, 0], \mathbb{R}^{4n}_+)$ at initial time $t_0 = 0$, where

$$\begin{aligned} \tau_M &:= \max\{\tau_{1(i)}, \tau_{2(i)}, \tau_{3(i)}, \tau_{4(i)}, 1 \le i \le n\}, \\ \mathbb{R}^{4n}_+ &:= \{(x_1, \cdots, x_{4n}) | x_j \ge 0, j = 1, \cdots, 4n\}. \end{aligned}$$

Let $\mathbb{X}(t; \phi)$ be the solution of (2.1) defined by $\mathbb{X}(t+\theta; \phi) = \Psi(t, \phi)(\theta)$, $\theta \in [-\tau_M, 0]$, for $t > 0$. We further denote $\mathbb{X}(t) = (\mathbf{x}_{(1)}(t), \cdots, \mathbf{x}_{(n)}(t)) = \mathbb{X}(t; \phi) = (\mathbf{x}_{(1)}(t; \phi), \cdots, \mathbf{x}_{(n)}(t; \phi))$, where $\mathbf{x}_{(i)} = (x_{1(i)}, x_{2(i)}, x_{3(i)}, x_{4(i)})$ for each i, if ϕ is not specified.

The basic dynamical properties for the system of two identical cells, i.e., $n = 2$ in (2.5), have been established in [19]. We present herein the extension of those properties to the general coupled n-cell system (2.1). The following two propositions, derived from the idea of sequential component-estimates, show that every solution $\mathbb{X}(t; \phi)$ of (2.1) exists and remains nonnegative for $t \in [0, \infty)$, for any initial condition $\phi \in \mathcal{C}([-\tau_M, 0], \mathbb{R}^{4n}_+)$, given any positive delays $\tau_{j(i)}$ and degradation rates $d_{j(i)}$, and other parameters. Their proofs resemble the ones for $n = 2$ in [19] and are omitted.

Proposition 2.1. *$\mathcal{C}([-\tau_M, 0], \mathbb{R}^{4n}_+)$ is positively invariant under the flow generated by system (2.1).*

Proposition 2.2. *There exists a compact set $\mathcal{Q} = \Pi_{i=1}^n (Q_{1(i)} \times Q_{2(i)} \times Q_{3(i)} \times Q_{4(i)}) \subset \mathbb{R}^{4n}_+$, such that $\mathbb{X}(t; \phi)$ converges to $\mathcal{Q}$ as $t \to \infty$, for arbitrary $\phi \in \mathcal{C}([-\tau_M, 0], \mathbb{R}^{4n}_+)$, where $Q_{1(i)}, Q_{2(i)}, Q_{3(i)}$, and $Q_{4(i)}$ are defined by*

$$\begin{aligned} Q_{1(i)} &= [\check{q}_{1(i)}, \hat{q}_{1(i)}] := [0, \tfrac{k_H}{d_{1(i)}}], \qquad Q_{2(i)} = [\check{q}_{2(i)}, \hat{q}_{2(i)}] := [0, \tfrac{a_2 k_H}{d_{1(i)} d_{2(i)}}], \\ Q_{3(i)} &= [\check{q}_{3(i)}, \hat{q}_{3(i)}] := [\tfrac{\check{c}_{3(i)}}{d_{3(i)}}, \tfrac{k_D}{d_{3(i)}}], \quad Q_{4(i)} = [\check{q}_{4(i)}, \hat{q}_{4(i)}] := [\tfrac{a_4 \check{c}_{3(i)}}{d_{3(i)} d_{4(i)}}, \tfrac{a_4 k_D}{d_{3(i)} d_{4(i)}}], \end{aligned}$$

and $\check{c}_{3(i)} := k_D P_0^2 / [P_0^2 + (\frac{a_2 k_H}{d_{1(i)} d_{2(i)}})^2]$, for $1 \le i \le n$.

2.1. **Oscillation-arrested.** In this subsection, we study the kinetics of gene expressions for the n cells located in the determined region. For the system of n non-identical cells (2.1), we shall show that their gene expressions tend to a non-uniform steady state corresponding to high and low expression levels as all degradation rates are large enough.

For the system of n identical cells, it is straightforward to verify that there exists a synchronous equilibrium. For system (2.1) of non-identical cells, we utilize the implicit function theorem to deduce the existence of an asynchronous equilibrium. We then employ the sequential-contracting technique and the Gauss-Seidel iteration to derive the criterion for the global convergence to this equilibrium. Such a dynamical scenario is linked to the state of oscillation-arrested for the cells at the DR.

First, analogous to the two-cell case in [19], there exists a positive synchronous equilibrium for the system (2.5) of n identical cells.

Proposition 2.3. *There exists a positive synchronous equilibrium point $\bar{\mathbb{X}} = (\bar{\mathbf{x}}, \cdots, \bar{\mathbf{x}})$ for system (2.5), where $\bar{\mathbf{x}} = (\bar{x}_1, \bar{x}_2, \bar{x}_3, \bar{x}_4)$,*

$$\bar{x}_1 = \frac{d_2 \bar{x}_2}{a_2}, \ \bar{x}_3 = \frac{k_D P_0^2}{d_3 (P_0^2 + \bar{x}_2^2)}, \ \bar{x}_4 = \frac{a_4 k_D P_0^2}{d_3 d_4 (P_0^2 + \bar{x}_2^2)},$$

and $\bar{x}_2$ is a positive solution to the equation:

$$P(\xi) := c_5\xi^5 + c_3\xi^3 - c_2\xi^2 + c_1\xi = a_2k_HP_0^4(d_3d_4P_{D_0} + a_4k_D),$$

with $c_1 := d_1d_2P_0^4(d_3d_4P_{D_0} + a_4k_D) > 0$, $c_2 := a_2d_3d_4k_HP_0^2P_{D_0} > 0$, $c_3 := 2d_1d_2d_3d_4P_0^2P_{D_0} > 0$, *and* $c_5 := d_1d_2d_3d_4P_{D_0} > 0$.

Proposition 2.3 follows from solving the stationary equations of (2.5). With the existence of the synchronous equilibrium $\bar{\mathbb{X}}$, we further define

$$\begin{gathered}\bar{\gamma}_1 := -\tfrac{\partial g_H}{\partial u}(u,v)|_{u=\bar{x}_2,v=\bar{x}_4} > 0,\ \bar{\gamma}_2 := \tfrac{\partial g_H}{\partial v}(u,v)|_{u=\bar{x}_2,v=\bar{x}_4} > 0,\\ \bar{\gamma}_3 := -\tfrac{dg_D}{du}(u)|_{u=\bar{x}_2} > 0,\end{gathered} \tag{2.6}$$

$$\begin{gathered}M_1 := \begin{pmatrix} -d_1 & -\bar{\gamma}_1 & 0 & 0\\ a_2 & -d_2 & 0 & 0\\ 0 & -\bar{\gamma}_3 & -d_3 & 0\\ 0 & 0 & a_4 & -d_4 \end{pmatrix}, M_2 := \begin{pmatrix} 0 & 0 & 0 & \bar{\gamma}_2\\ 0 & 0 & 0 & 0\\ 0 & 0 & 0 & 0\\ 0 & 0 & 0 & 0 \end{pmatrix},\\ M_3 := \begin{pmatrix} 0 & 0 & 0 & \bar{\gamma}_2/2\\ 0 & 0 & 0 & 0\\ 0 & 0 & 0 & 0\\ 0 & 0 & 0 & 0 \end{pmatrix},\end{gathered} \tag{2.7}$$

$$M := \begin{pmatrix} M_1 & M_2 & 0 & \cdots & \cdots & 0\\ M_3 & M_1 & M_3 & \ddots & & \vdots\\ 0 & M_3 & M_1 & M_3 & \ddots & \vdots\\ \vdots & \ddots & \ddots & \ddots & \ddots & 0\\ \vdots & & \ddots & M_3 & M_1 & M_3\\ 0 & \cdots & \cdots & 0 & M_2 & M_1 \end{pmatrix}_{4n\times 4n}. \tag{2.8}$$

We derive the existence of equilibrium for system of non-identical cells (2.1) as follows. Let $\mathrm{int}(\mathbb{R}_+^{4n})$ denote the interior of $\mathbb{R}_+^{4n}$.

Proposition 2.4. *For given degradation rate* $\bar{\mathbf{d}} := (d_1, d_2, d_3, d_4, \cdots, d_1, d_2, d_3, d_4) \in \mathrm{int}(\mathbb{R}_+^{4n})$ *for system* (2.5) *and other fixed parameters and delays in* (2.5), *if*

$$\det(M) \neq 0, \tag{2.9}$$

then system (2.1) *admits a positive equilibrium point* $\mathbb{X}^* = (\mathbf{x}_{(1)}^*, \mathbf{x}_{(2)}^*, \cdots, \mathbf{x}_{(n)}^*)$ *with* $\mathbf{x}_{(i)}^* = (x_{1(i)}^*,\ x_{2(i)}^*,\ x_{3(i)}^*,\ x_{4(i)}^*)$, $i = 1, 2, \cdots, n$, *provided that the degradation rate* $(d_{1(1)},\ d_{2(1)},\ d_{3(1)},\ d_{4(1)}, \cdots, d_{1(n)},\ d_{2(n)},\ d_{3(n)},\ d_{4(n)})$ *is close to* $\bar{\mathbf{d}}$.

Proof. We define a function $F : \mathbb{R}^{8n} \to \mathbb{R}^{4n}$ by $F(\mathbf{X}, \mathbf{d}) = (F_1(\mathbf{X}, \mathbf{d}), F_2(\mathbf{X}, \mathbf{d}), \cdots, F_{4n}(\mathbf{X}, \mathbf{d}))$ with

$$\begin{aligned} F_{4(i-1)+1}(\mathbf{X}, \mathbf{d}) &:= g_H(x_{2(i)}, \tilde{x}_{4(i)}) - d_{1(i)}x_{1(i)},\\ F_{4(i-1)+2}(\mathbf{X}, \mathbf{d}) &:= a_2x_{1(i)} - d_{2(i)}x_{2(i)},\\ F_{4(i-1)+3}(\mathbf{X}, \mathbf{d}) &:= g_D(x_{2(i)}) - d_{3(i)}x_{3(i)},\\ F_{4i}(\mathbf{X}, \mathbf{d}) &:= a_4x_{3(i)} - d_{4(i)}x_{4(i)}, \end{aligned}$$

for $\mathbf{X} = (\mathbf{x}_{(1)},\ \mathbf{x}_{(2)}, \cdots, \mathbf{x}_{(n)})$ and $\mathbf{d} = (\mathbf{d}_{(1)},\ \mathbf{d}_{(2)}, \cdots, \mathbf{d}_{(n)})$ with $\mathbf{x}_{(i)} = (x_{1(i)},\ x_{2(i)},\ x_{3(i)},\ x_{4(i)})$ and $\mathbf{d}_{(i)} = (d_{1(i)},\ d_{2(i)},\ d_{3(i)},\ d_{4(i)})$, for $i = 1, 2, \cdots, n$. For any

$\bar{\mathbf{d}} = (d_1, d_2, d_3, d_4, \cdots, d_1, d_2, d_3, d_4) \in \text{int}(\mathbb{R}^{4n}_+)$, there exists $\bar{\mathbb{X}} \in \text{int}(\mathbb{R}^{4n}_+)$ such that $F(\bar{\mathbb{X}}, \bar{\mathbf{d}}) = 0$, thanks to Proposition 2.3. According to (2.9), we have

$$J = |\frac{\partial F_k}{\partial x_\ell}|_{(\mathbf{X},\mathbf{d})=(\bar{\mathbb{X}},\bar{\mathbf{d}})} \neq 0, \text{ for } k, \ell = 1, 2, \cdots, 4n;$$

therefore, by the implicit function theorem, if $\mathbf{d}$ is close to $\bar{\mathbf{d}}$, then there exists a positive equilibrium $\mathbb{X}^* = (\mathbf{x}^*_{(1)}, \mathbf{x}^*_{(2)}, \cdots, \mathbf{x}^*_{(n)})$ close to $\bar{\mathbb{X}}$ such that $F(\mathbb{X}^*, \mathbf{d}) = 0$. □

Remark 2.1. (i) If system (2.1) is designated for n non-identical cells, then the positive equilibrium $\mathbb{X}^*$ in Proposition 2.4 is asynchronous in general, see Example 2.1. (ii) For $n = 2$, the condition (2.9) can be replaced by $d_1d_2d_3d_4 + a_2\bar{\gamma}_1d_3d_4 - a_2a_4\bar{\gamma}_2\bar{\gamma}_3 \neq 0$.

While system (2.1) admits an equilibrium $\mathbb{X}^*$, we can discuss the global convergence to $\mathbb{X}^*$. Let us translate system (2.1) from $\mathbb{X}^*$ to the origin, and retain the same notation:

$$\begin{cases} \dot{x}_{1(i)}(t) = -d_{1(i)}x_{1(i)}(t) - d_{1(i)}x^*_{1(i)} \\ \qquad\qquad +g_{H(i)}(x_{2(i)}(t-\tau_{1(i)}) + x^*_{2(i)}, \tilde{x}_{4(i)}(t-\tau_{1(i)}) + \tilde{x}^*_{4(i)}) \\ \dot{x}_{2(i)}(t) = -d_{2(i)}x_{2(i)}(t) + a_2x_{1(i)}(t-\tau_{2(i)}) \\ \dot{x}_{3(i)}(t) = -d_{3(i)}x_{3(i)}(t) - d_{3(i)}x^*_{3(i)} + g_D(x_{2(i)}(t-\tau_{3(i)}) + x^*_{2(i)}) \\ \dot{x}_{4(i)}(t) = -d_{4(i)}x_{4(i)}(t) + a_4x_{3(i)}(t-\tau_{4(i)}), \end{cases} \tag{2.10}$$

where $1 \leq i \leq n$ and $\tilde{x}^*_{4(i)} = [x^*_{4(i-1)} + x^*_{4(i+1)}]/2$, for $i = 2, \cdots, n-1$ and $\tilde{x}^*_{4(1)} = x^*_{4(2)}$, $\tilde{x}^*_{4(n)} = x^*_{4(n-1)}$. Note that after the translation, $\mathbb{X}(t)$ eventually converges to $\mathcal{Q} - \mathbb{X}^* = \Pi_{i=1}^n(Q^*_{1(i)} \times Q^*_{2(i)} \times Q^*_{3(i)} \times Q^*_{4(i)})$, as $t \to \infty$, where $Q^*_{j(i)} := [\check{q}_{j(i)} - x^*_{j(i)}, \hat{q}_{j(i)} - x^*_{j(i)}]$, for $j = 1, 2, 3, 4$ and $i = 1, 2, \cdots, n$.

We shall show that every solution of system (2.10) converges to the origin, as $t \to \infty$. By the mean value theorem, we put each component of (2.10) in the form

$$\dot{x}_{j(i)}(t) = -d_{j(i)}x_{j(i)}(t) + w_{j(i)}(t), \ j = 1, 2, 3, 4, \ 1 \leq i \leq n, \tag{2.11}$$

where

$$\begin{aligned} w_{1(1)}(t) &:= \frac{\partial g_H}{\partial u}(u_{(1)}, v_{(1)}) \cdot x_{2(1)}(t-\tau_{1(1)}) + \frac{\partial g_H}{\partial v}(u_{(1)}, v_{(1)}) \cdot x_{4(2)}(t-\tau_{1(1)}), \\ w_{1(i)}(t) &:= \frac{\partial g_H}{\partial u}(u_{(i)}, v_{(i)}) \cdot x_{2(i)}(t-\tau_{1(i)}) \\ &\quad + \frac{\partial g_H}{\partial v}(u_{(i)}, v_{(i)}) \cdot [x_{4(i-1)}(t-\tau_{1(i)}) + x_{4(i+1)}(t-\tau_{1(i)})]/2, \\ &\qquad\qquad \text{for } i = 2, \cdots, n-1, \\ w_{1(n)}(t) &:= \frac{\partial g_H}{\partial u}(u_{(n)}, v_{(n)}) \cdot x_{2(n)}(t-\tau_{1(n)}) + \frac{\partial g_H}{\partial v}(u_{(n)}, v_{(n)}) \cdot x_{4(n-1)}(t-\tau_{1(n)}), \end{aligned}$$

and for $1 \leq i \leq n$,

$$\begin{aligned} w_{2(i)}(t) &:= a_2x_{1(i)}(t-\tau_{2(i)}), \\ w_{3(i)}(t) &:= \tfrac{dg_D}{du}(\eta_{(i)}) \cdot x_{2(i)}(t-\tau_{3(i)}), \\ w_{4(i)}(t) &:= a_4x_{3(i)}(t-\tau_{4(i)}), \end{aligned}$$

with $u_{(i)} := u_{(i)}(t-\tau_{1(i)})$ (resp., $\eta_{(i)} := \eta_{(i)}(t-\tau_{3(i)})$) lying between $x_{2(i)}(t-\tau_{1(i)}) + x^*_{2(i)}$ and $x^*_{2(i)}$ (resp., $x_{2(i)}(t-\tau_{3(i)}) + x^*_{2(i)}$ and $x^*_{2(i)}$) and $v_{(i)} := v_{(i)}(t-\tau_{1(i)})$ between $x_{4(2)}(t-\tau_{1(1)}) + x^*_{4(2)}$ and $x^*_{4(2)}$, $(x_{4(i-1)}(t-\tau_{1(i)}) + x_{4(i+1)}(t-\tau_{1(i)}) + x^*_{4(i-1)} +$

$x^*_{4(i+1)})/2$ and $(x^*_{4(i-1)} + x^*_{4(i+1)})/2$, and $x_{4(n-1)}(t-\tau_{1(n)}) + x^*_{4(n-1)}$ and $x^*_{4(n-1)}$, for $i = 1$, $i = 2, 3, \cdots, n-1$, and $i = n$, respectively.

It can be shown that there exist $4n$ intervals $I_{j(i)} := [-\delta_{j(i)}, \delta_{j(i)}]$ to which the $(4i + j - 4)$th component of $\mathbb{X}(t)$ converges respectively, for $j = 1, 2, 3, 4$ and $1 \le i \le n$. Moreover, the lengths of the intervals can be estimated as

$$0 \le \delta_{j(i)} \le |w_{j(i)}|^{\max}(\infty)/d_{j(i)}, \tag{2.12}$$

where $|w_{j(i)}|^{\max}(t) := \sup\{|w_{j(i)}(s)| : s \ge t\}$, and
$|w_{j(i)}|^{\max}(\infty) := \lim_{t\to\infty} |w_{j(i)}|^{\max}(t)$, for $j = 1, 2, 3, 4$, $1 \le i \le n$; cf. [27, 28]. Let us define

$$\begin{aligned}
&\rho_{1(1)} := \max_{u\in Q_{2(1)},\ v\in Q_{4(2)}} \{|\frac{\partial g_H(u,v)}{\partial u}|\},\ \rho_{2(1)} := \max_{u\in Q_{2(1)},\ v\in Q_{4(2)}} \{|\frac{\partial g_H(u,v)}{\partial v}|\},\\
&\rho_{1(i)} := \max_{u\in Q_{2(i)},\ v\in \tilde{Q}_{4(i)}} \{|\frac{\partial g_H(u,v)}{\partial u}|\},\ \rho_{2(i)} := \max_{u\in Q_{2(i)},\ v\in \tilde{Q}_{4(i)}} \{|\frac{\partial g_H(u,v)}{\partial v}|\},\\
&\qquad\qquad\qquad\qquad\qquad\qquad\qquad\qquad\qquad\qquad \text{for } 1 < i < n,\\
&\rho_{1(n)} := \max_{u\in Q_{2(n)},\ v\in Q_{4(n-1)}} \{|\frac{\partial g_H(u,v)}{\partial u}|\},\ \rho_{2(n)} := \max_{u\in Q_{2(n)},\ v\in Q_{4(n-1)}} \{|\frac{\partial g_H(u,v)}{\partial v}|\},\\
&\rho_{3(i)} := \max_{u\in Q_{2(i)}} \{|\frac{dg_D(u)}{du}|\},\ \text{for } 1 \le i \le n,
\end{aligned} \tag{2.13}$$

where $\tilde{Q}_{4(i)} := [(\check{q}_{4(i-1)} + \check{q}_{4(i+1)})/2, (\hat{q}_{4(i-1)} + \hat{q}_{4(i+1)})/2]$, for $1 < i < n$.

Now, we present the main result of this subsection.

Theorem 2.5. *Assume that an equilibrium $\mathbb{X}^*$ of system (2.1) exists. Then every solution of (2.1) converges to the equilibrium $\mathbb{X}^*$ provided*

$$d_{1(i)} > \rho_{1(i)} + \rho_{2(i)},\ d_{2(i)} > a_2,\ d_{3(i)} > \rho_{3(i)},\ d_{4(i)} > a_4, \tag{2.14}$$

for all $i = 1, 2, \cdots, n$.

Proof. By utilizing the estimate in (2.12) to each component in (2.11) successively, it can be shown that there exists a sequence of estimates for $\delta_{j(i)}$, namely, $\delta_{j(i)} \le \delta^{(k)}_{j(i)}$, $j = 1, 2, 3, 4$, $i = 1, \cdots, n$, where for each $k \in \mathbb{N}$,

$$\begin{aligned}
0 \le \delta^{(k)}_{1(i)} &:= \begin{cases} (\rho_{1(1)}\delta^{(k-1)}_{2(1)} + \rho_{2(1)}\delta^{(k-1)}_{4(2)})/d_{1(1)}, & \text{if } i = 1,\\ (\rho_{1(i)}\delta^{(k-1)}_{2(i)} + \rho_{2(i)}(\delta^{(k)}_{4(i-1)} + \delta^{(k-1)}_{4(i+1)})/2)/d_{1(i)}, & \text{if } 1 < i < n,\\ (\rho_{1(n)}\delta^{(k-1)}_{2(n)} + \rho_{2(n)}\delta^{(k)}_{4(n-1)})/d_{1(n)}, & \text{if } i = n, \end{cases}\\
0 \le \delta^{(k)}_{2(i)} &:= (a_2/d_{2(i)})\delta^{(k)}_{1(i)},\\
0 \le \delta^{(k)}_{3(i)} &:= (\rho_{3(i)}/d_{3(i)})\delta^{(k)}_{2(i)},\\
0 \le \delta^{(k)}_{4(i)} &:= (a_4/d_{4(i)})\delta^{(k)}_{3(i)},
\end{aligned} \tag{2.15}$$

and $\delta^{(0)}_{2(i)} := \max\{|\check{q}_{2(i)} - x^*_{2(i)}|, |\hat{q}_{2(i)} - x^*_{2(i)}|\}$, $\delta^{(0)}_{4(i)} := \max\{|\check{q}_{4(i)} - x^*_{4(i)}|, |\hat{q}_{4(i)} - x^*_{4(i)}|\}$, with $\rho_{1(i)}$, $\rho_{2(i)}$, and $\rho_{3(i)}$ defined in (2.13). Moreover, the $(4i + j - 4)$th component for the solution $\mathbb{X}(t)$ of system (2.10) converges to $I^{(k)}_{j(i)} := [-\delta^{(k)}_{j(i)}, \delta^{(k)}_{j(i)}]$, as $t \to \infty$, for all $k \in \mathbb{N}$. The detailed arguments are similar to those in [19]. From the iterative estimates (2.15), we observe that the sequence $\{\delta^{(k)}_{j(i)} | j = 1, 2, 3, 4,\ 1 \le$

$i \le n, k \in \mathbb{N}\}$ is in the form of the Gauss-Seidel iteration for solving the linear system

$$(\mathbf{ML}+\mathbf{E})\mathbf{y} = 0,$$

where $\mathbf{M} := [m_{pq}]_{1\le p,q\le 4n}$ with

$$\begin{aligned}
&m_{4(p-1)+2,4(p-1)+1} = -a_2,\ m_{4p,4(p-1)+3} = -a_4,\ \text{for } 1 \le p \le n,\\
&m_{4(p-1)+1,4(p-1)+2} = -\rho_{1(p)},\ m_{4(p-1)+3,4(p-1)+2} = -\rho_{3(p)},\ \text{for } 1 \le p \le n,\\
&m_{4p+1,4p} = m_{4p+1,4(p+2)} = -\rho_{2(p+1)}/2,\ \text{for } 1 \le p \le n-2,\\
&m_{1,8} = -\rho_{2(1)},\ m_{4(n-1)+1,4(n-1)} = -\rho_{2(n)},\\
&m_{pq} = 0,\ \text{otherwise},
\end{aligned}$$

$$\begin{aligned}
\mathbf{L} &:= I_{4n\times 4n},\\
\mathbf{E} &:= \operatorname{diag}\{d_{1(1)}, d_{2(1)}, d_{3(1)}, d_{4(1)}, \cdots, d_{1(n)}, d_{2(n)}, d_{3(n)}, d_{4(n)}\}.
\end{aligned}$$

Since $\mathbf{ML}+\mathbf{E}$ is strictly diagonal-dominant under condition (2.14) (cf. [27, 33]), we obtain $\delta_{j(i)}^{(k)} \to 0$, as $k \to \infty$, for each $1 \le j \le 4$ and $1 \le i \le n$. □

Remark 2.2. (i) Theorem 2.5 shall be adopted to indicate that if the cells located in the DR have large degradation rates, then the gene expressions of *her* and *delta* in these cells eventually converge to some steady state $\mathbb{X}^*$. For non-identical cells (with different degradation rates) in this region, $\mathbb{X}^*$ is non-uniform among different cells. We shall present an example below to show high and low expressions in the components of $\mathbb{X}^*$, which correspond to the anterior and posterior of a formed somite. We interpret this scenario as that when the peak and foot of the oscillatory wave arrive at the anterior end of the TWR, there generate distinct reactions which vary the degradation rates and form high and low expression levels, respectively.
(ii) If we consider system (2.5) of n identical cells, then there exist an attracting set $\mathcal{Q} = (\Pi_{i=1}^4 Q_i)^n \subset \mathbb{R}_+^{4n}$, with

$$\begin{aligned}
Q_1 &= [\check{q}_1, \hat{q}_1] := [0, k_H/d_1], \qquad Q_2 = [\check{q}_2, \hat{q}_2] := [0, a_2 k_H/(d_1 d_2)],\\
Q_3 &= [\check{q}_3, \hat{q}_3] := [\check{c}_3/d_3, k_D/d_3], \quad Q_4 = [\check{q}_4, \hat{q}_4] := [a_4\check{c}_3/(d_3 d_4), a_4 k_D/(d_3 d_4)],
\end{aligned}$$

where $\check{c}_3 := k_D P_0^2/[P_0^2 + (\frac{a_2 k_H}{d_1 d_2})^2]$, and a positive synchronous equilibrium $\bar{\mathbb{X}}$, thanks to Proposition 2.3. By applying arguments analogous to the ones in Theorem 2.5, it can be shown that every solution of system (2.5) converges to the synchronous equilibrium $\bar{\mathbb{X}}$, provided

$$\hat{\rho}_1 a_2 d_3 d_4 + \hat{\rho}_2 \hat{\rho}_3 a_2 a_4 < d_1 d_2 d_3 d_4, \tag{2.16}$$

where $\hat{\rho}_1 := \frac{2k_H P_{D_0} \hat{q}_2 (P_{D_0} + \hat{q}_4)}{P_0^2 (P_{D_0} + \check{q}_4)^2}$, $\hat{\rho}_2 := \frac{k_H P_{D_0} \hat{q}_2^2}{P_0^2 (P_{D_0} + \check{q}_4)^2}$, and $\hat{\rho}_3 := \frac{2a_2 k_D k_H}{P_0^2 d_1 d_2}$. Note that condition (2.16) is weaker than condition (2.14), and the assertion reveals that the gene expressions eventually tend to a uniform steady state $\bar{\mathbb{X}}$.

The following example shows the existence of an asynchronous equilibrium in the system of two non-identical cells.

Example 2.1. We consider the system of two non-identical cells, i.e., system (2.1) with $n = 2$; we set

$$a_2 = a_4 = 4.5,\ k_H = k_D = 33,\ P_0 = 40,\ P_{D_0} = 400.$$

First, if these two cells have close degradation rates

$$d_{1(1)} = 2.3,\ d_{2(1)} = 4.1,\ d_{3(1)} = 2.3,\ d_{4(1)} = 4.1,$$
$$d_{1(2)} = 2.31,\ d_{2(2)} = 4.2,\ d_{3(2)} = 2.29,\ d_{4(2)} = 4.2,$$

then the system admits an asynchronous equilibrium

$$\mathbb{X}^* \approx (12.82,\ 14.07,\ 12.77,\ 14.01,\ 12.82,\ 13.74,\ 12.89,\ 13.81),$$

and solutions tend to this equilibrium $\mathbb{X}^*$ if the initial value is close to $\mathbb{X}^*$.

Next, if we set the degradation rates of these two cells apart from each other, and satisfy condition (2.14):

$$d_{1(1)} = 2.3,\ d_{2(1)} = 5,\ d_{3(1)} = 2.3,\ d_{4(1)} = 5,$$
$$d_{1(2)} = 4,\ d_{2(2)} = 4.6,\ d_{3(2)} = 4,\ d_{4(2)} = 4.6,$$

then the system admits a globally stable asynchronous equilibrium

$$\mathbb{X}^* \approx (13.2,\ 11.88,\ 13.18,\ 11.87,\ 7.96,\ 7.78,\ 7.95,\ 7.78).$$

Note that the gene expression of cell 1 (resp., cell 2) tends to a higher level (resp., lower level) of expression which corresponds to the anterior (resp., posterior) of a somite, as these two cells are located at the DR.

2.2. **Oscillations.** In zebrafish embryo, clock genes for the cells at the TB show synchronous oscillations with period about 30 minutes. Such a scenario can be depicted by considering coupled system (2.5) of n identical cells. Employing the delay Hopf bifurcation theory to establish synchronous periodic solutions has been completed for the two-cell case in [19]. Note that the synchronous manifold

$$\mathcal{S} := \{(\mathbf{x}_{(1)}, \cdots, \mathbf{x}_{(n)}) : \mathbf{x}_{(i)} = \mathbf{x}_{(1)} \in \mathcal{C}([-\tau_M, 0], \mathbb{R}^4_+),\ \text{for all } i = 2, \cdots, n\}$$

is positively invariant under the flow generated by system (2.5). Therefore, we can consider the dynamics of (2.5) restricted to $\mathcal{S}$:

$$\begin{cases} \dot{x}_1(t) &= g_H(x_2(t-\tau_1),\ x_4(t-\tau_1)) - d_1 x_1(t) \\ \dot{x}_2(t) &= a_2 x_1(t-\tau_2) - d_2 x_2(t) \\ \dot{x}_3(t) &= g_D(x_2(t-\tau_3)) - d_3 x_3(t) \\ \dot{x}_4(t) &= a_4 x_3(t-\tau_4) - d_4 x_4(t). \end{cases} \tag{2.17}$$

The computation and analysis for the two-cell case in [19] can then be adapted to the n-cell system (2.5).

On the other hand, oscillatory wave of gene expression traveling from the posterior end to the anterior end in the TWR has been observed in experiments. This spatiotemporal pattern indicates that gene expressions for the cells at the TWR remain oscillatory. These oscillations are out of synchrony, but sustain a suitable spatiotemporal pace, so that the peaks of oscillations can move anteriorly without collision.

In this subsection, we consider the cells located in the TWR with different degradation rates, and show that such asynchronous oscillation can be generated. We also illustrate that cell with larger degradation rate has smaller amplitude of oscillation. For simplicity, we consider the coupled system of two cells with different

degradation rates

$$\begin{cases} \dot{x}_{1(1)}(t) &= g_H(x_{2(1)}(t-\tau_1), x_{4(2)}(t-\tau_1)) - d_{1(1)}x_{1(1)}(t) \\ \dot{x}_{2(1)}(t) &= a_2 x_{1(1)}(t-\tau_2) - d_{2(1)}x_{2(1)}(t) \\ \dot{x}_{3(1)}(t) &= g_D(x_{2(1)}(t-\tau_3)) - d_{3(1)}x_{3(1)}(t) \\ \dot{x}_{4(1)}(t) &= a_4 x_{3(1)}(t-\tau_4) - d_{4(1)}x_{4(1)}(t) \\ \dot{x}_{1(2)}(t) &= g_H(x_{2(2)}(t-\tau_1), x_{4(1)}(t-\tau_1)) - d_{1(2)}x_{1(2)}(t) \\ \dot{x}_{2(2)}(t) &= a_2 x_{1(2)}(t-\tau_2) - d_{2(2)}x_{2(2)}(t) \\ \dot{x}_{3(2)}(t) &= g_D(x_{2(2)}(t-\tau_3)) - d_{3(2)}x_{3(2)}(t) \\ \dot{x}_{4(2)}(t) &= a_4 x_{3(2)}(t-\tau_4) - d_{4(2)}x_{4(2)}(t), \end{cases} \tag{2.18}$$

where $d_{j(1)} \neq d_{j(2)}$, for some $j \in \{1,2,3,4\}$. Note that the synchronous manifold $\mathcal{S}$ is no longer positively invariant under system (2.18). Our goal is to employ delay Hopf bifurcation theory to explore the existence of asynchronous periodic solution for system (2.18).

Following the discussions in section 2, we assume that system (2.18) has an asynchronous equilibrium $\mathbb{X}^* = (\mathbf{x}^*_{(1)}, \mathbf{x}^*_{(2)})$. We then translate system (2.18) from $\mathbb{X}^*$ to the origin; the linearized system at the origin is

$$\begin{cases} \dot{x}_{1(1)}(t) &= -d_{1(1)}x_{1(1)}(t) + \ell_{11}x_{2(1)}(t-\tau_1) + \ell_{12}x_{4(2)}(t-\tau_1) \\ \dot{x}_{2(1)}(t) &= -d_{2(1)}x_{2(1)}(t) + a_2 x_{1(1)}(t-\tau_2) \\ \dot{x}_{3(1)}(t) &= -d_{3(1)}x_{3(1)}(t) + \ell_{31}x_{2(1)}(t-\tau_3) \\ \dot{x}_{4(1)}(t) &= -d_{4(1)}x_{4(1)}(t) + a_4 x_{3(1)}(t-\tau_4) \\ \dot{x}_{1(2)}(t) &= -d_{1(2)}x_{1(2)}(t) + \ell_{51}x_{2(2)}(t-\tau_1) + \ell_{52}x_{4(1)}(t-\tau_1) \\ \dot{x}_{2(2)}(t) &= -d_{2(2)}x_{2(2)}(t) + a_2 x_{1(2)}(t-\tau_2) \\ \dot{x}_{3(2)}(t) &= -d_{3(2)}x_{3(2)}(t) + \ell_{71}x_{2(2)}(t-\tau_3) \\ \dot{x}_{4(2)}(t) &= -d_{4(2)}x_{4(2)}(t) + a_4 x_{3(2)}(t-\tau_4), \end{cases} \tag{2.19}$$

where

$$\begin{array}{lll} \ell_{11} := \frac{\partial g_H}{\partial u}(x^*_{2(1)}, x^*_{4(2)}), & \ell_{12} := \frac{\partial g_H}{\partial v}(x^*_{2(1)}, x^*_{4(2)}), & \ell_{31} := \frac{dg_D}{du}(x^*_{2(1)}), \\ \ell_{51} := \frac{\partial g_H}{\partial u}(x^*_{2(2)}, x^*_{4(1)}), & \ell_{52} := \frac{\partial g_H}{\partial v}(x^*_{2(2)}, x^*_{4(1)}), & \ell_{71} := \frac{dg_D}{du}(x^*_{2(2)}). \end{array} \tag{2.20}$$

For convenience, we set $\gamma_1 = -\ell_{11}$, $\gamma_2 = \ell_{12}$, $\gamma_3 = -\ell_{31}$, $\gamma_4 = -\ell_{51}$, $\gamma_5 = \ell_{52}$, $\gamma_6 = -\ell_{71}$ and $\gamma_i > 0$, $i = 1, 2, \cdots, 6$.

The characteristic equation for (2.19) is given by

$$0 = \triangle(\lambda, \tau_1, \tau_2, \tau_3, \tau_4) := \det \begin{pmatrix} A_{(1)} & B_{(1)} \\ B_{(2)} & A_{(2)} \end{pmatrix}, \tag{2.21}$$

where

$$A_{(1)} := \begin{pmatrix} \lambda + d_{1(1)} & \gamma_1 e^{-\tau_1\lambda} & 0 & 0 \\ -a_2 e^{-\tau_2\lambda} & \lambda + d_{2(1)} & 0 & 0 \\ 0 & \gamma_3 e^{-\tau_3\lambda} & \lambda + d_{3(1)} & 0 \\ 0 & 0 & -a_4 e^{-\tau_4\lambda} & \lambda + d_{4(1)} \end{pmatrix}, B_{(1)} := \begin{pmatrix} 0 & 0 & 0 & -\gamma_2 e^{-\tau_1\lambda} \\ 0 & 0 & 0 & 0 \\ 0 & 0 & 0 & 0 \\ 0 & 0 & 0 & 0 \end{pmatrix},$$

$$A_{(2)} := \begin{pmatrix} \lambda + d_{1(2)} & \gamma_4 e^{-\tau_1\lambda} & 0 & 0 \\ -a_2 e^{-\tau_2\lambda} & \lambda + d_{2(2)} & 0 & 0 \\ 0 & \gamma_6 e^{-\tau_3\lambda} & \lambda + d_{3(2)} & 0 \\ 0 & 0 & -a_4 e^{-\tau_4\lambda} & \lambda + d_{4(2)} \end{pmatrix}, B_{(2)} := \begin{pmatrix} 0 & 0 & 0 & -\gamma_5 e^{-\tau_1\lambda} \\ 0 & 0 & 0 & 0 \\ 0 & 0 & 0 & 0 \\ 0 & 0 & 0 & 0 \end{pmatrix}.$$

We compute to obtain

$$\begin{aligned} & \triangle(\lambda,\tau_1,\tau_2,\tau_3,\tau_4) \\ = \; & \lambda^8+\beta_7\lambda^7+\beta_6\lambda^6+\beta_5\lambda^5+\beta_4\lambda^4+\beta_3\lambda^3+\beta_2\lambda^2+\beta_1\lambda+\beta_0 \\ & +e^{-(\tau_1+\tau_2)\lambda}(\alpha_{16}\lambda^6+\alpha_{15}\lambda^5+\alpha_{14}\lambda^4+\alpha_{13}\lambda^3+\alpha_{12}\lambda^2+\alpha_{11}\lambda+\alpha_{10}) \\ & +e^{-2(\tau_1+\tau_2)\lambda}(\alpha_{24}\lambda^4+\alpha_{23}\lambda^3+\alpha_{22}\lambda^2+\alpha_{21}\lambda+\alpha_{20})-e^{-2(\tau_1+\tau_2+\tau_3+\tau_4)\lambda}\alpha_{30}, \end{aligned}$$

where α_{ij} and β_i are positive constants. We set $r:=\tau_1+\tau_2$, $s:=\tau_3+\tau_4$, and write $\triangle(\lambda,\tau_1,\tau_2,\tau_3,\tau_4)=\triangle(\lambda,r,s)$. To employ the bifurcation theory, we take r as a bifurcation parameter, while holding s fixed. Finding purely imaginary roots iw to the characteristic equation (2.21) can be proceeded by solving

$$e^{\lambda r}\cdot\triangle(\lambda,r,s)=0. \tag{2.22}$$

The real and imaginary parts of equation (2.22) read as

$$\begin{cases} \mathrm{Re}(w;r):=A_0(w)+A_{1s}(w)\cos(rw)+A_{2s}(w)\sin(rw)=0 \\ \mathrm{Im}(w;r):=B_0(w)+B_{1s}(w)\cos(rw)+B_{2s}(w)\sin(rw)=0, \end{cases} \tag{2.23}$$

where

$$\begin{aligned} A_0(w) &:= -\alpha_{16}w^6+\alpha_{14}w^4-\alpha_{12}w^2+\alpha_{10}, \\ A_{1s}(w) &:= w^8-\beta_6w^6+(\alpha_{24}+\beta_4)w^4-(\alpha_{22}+\beta_2)w^2+(\alpha_{20}+\beta_0) \\ &\quad -\alpha_{30}\cos(2sw), \\ A_{2s}(w) &:= \beta_7w^7-\beta_5w^5+(-\alpha_{23}+\beta_3)w^3+(\alpha_{21}-\beta_1)w+\alpha_{30}\sin(2sw), \\ B_0(w) &:= \alpha_{15}w^5-\alpha_{13}w^3+\alpha_{11}w, \\ B_{1s}(w) &:= -\beta_7w^7+\beta_5w^5-(\alpha_{23}+\beta_3)w^3+(\alpha_{21}+\beta_1)w+\alpha_{30}\sin(2sw), \\ B_{2s}(w) &:= w^8-\beta_6w^6+(-\alpha_{24}+\beta_4)w^4+(\alpha_{22}-\beta_2)w^2+(-\alpha_{20}+\beta_0) \\ &\quad +\alpha_{30}\cos(2sw). \end{aligned}$$

For any fixed $s\geq 0$, we define

$$\begin{aligned} P_0(w) &:= A_{2s}(w)B_{1s}(w)-A_{1s}(w)B_{2s}(w), \\ P_1(w) &:= A_0(w)B_{2s}(w)-A_{2s}(w)B_0(w), \\ P_2(w) &:= A_{1s}(w)B_0(w)-A_0(w)B_{1s}(w), \end{aligned}$$

and set

$$\begin{aligned} & Q_1(w):=P_1^2(w)+P_2^2(w),\ Q_2(w):=P_0^2(w),\ \text{for } w\in\mathbb{R}, \\ & Q(w):=Q_2(w)-Q_1(w),\ \text{for } w\in\mathbb{R}. \end{aligned}$$

We derive the criterion for the existence of purely imaginary eigenvalue iw_* and the corresponding bifurcation values $\{r_*^{(k)}(w_*)\}_{k\in\mathbb{Z}}$ in the following lemma.

Lemma 2.6. *If*

$$(-\alpha_{20}+\alpha_{30}+\beta_0)^2(\alpha_{20}-\alpha_{30}+\beta_0)^2<\alpha_{10}^2(-\alpha_{20}+\alpha_{30}+\beta_0)^2, \tag{2.24}$$

then $Q(\cdot)=0$ has at least one positive root w_*. Moreover, if

$$w_*\in U:=\{w\in\mathbb{R}:Q(w)=0\}/\{w\in\mathbb{R}:P_0(w)=0\}, \tag{2.25}$$

then there exists a corresponding sequence $\{r_*^{(k)}(w_*)\}_{k\in\mathbb{Z}}$ *defined by*

$$r_*^{(k)}(w_*) := \begin{cases} \frac{1}{w_*}[\tan^{-1}(\frac{S(w_*)}{C(w_*)}) + 2k\pi], & \text{if } C(w_*) > 0, \\ \frac{1}{w_*}[\tan^{-1}(\frac{S(w_*)}{C(w_*)}) + (2k-1)\pi], & \text{if } C(w_*) < 0, \\ \frac{1}{w_*}[\frac{3\pi}{2} + 2k\pi], & \text{if } C(w_*) = 0,\ S(w_*) < 0\ , \\ \frac{1}{w_*}[\frac{\pi}{2} + 2k\pi], & \text{if } C(w_*) = 0,\ S(w_*) > 0, \end{cases} \tag{2.26}$$

such that w_* *and* $r_*^{(k)}(w_*)$ *satisfy* $\triangle(iw_*, r_*^{(k)}(w_*), s) = 0$, *for* $k \in \mathbb{Z}$, *where*

$$C(w) := P_1(w)/P_0(w),\ S(w) := P_2(w)/P_0(w),\ \text{for } w \in U.$$

Proof. Since the leading term of $Q(w)$ is w^{32} and $Q(0) = (-\alpha_{20}+\alpha_{30}+\beta_0)^2(-\alpha_{10}^2+(\alpha_{20}-\alpha_{30}+\beta_0)^2)$, through arguments similar to those in [19], we derive the existence of solution w_* to $Q(\cdot) = 0$ under condition (2.24). Next, according to (2.25), we can further define

$$C(w) := P_1(w)/P_0(w),\ S(w) := P_2(w)/P_0(w),\ \text{for } w \in U,$$

such that $C^2(w_*) + S^2(w_*) = 1$, for all $w_* \in U$, due to $Q(w_*) = 0$. Moreover, taking $\cos(rw) = C(w_*)$ and $\sin(rw) = S(w_*)$ with $w = w^*$ and r defined by (2.26) into (2.23) yields $\mathrm{Re}(w_*; r_*^{(k)}(w_*)) = 0$ and $\mathrm{Im}(w_*; r_*^{(k)}(w_*)) = 0$. Hence, $\triangle(iw_*, r_*^{(k)}(w_*), s) = 0$, for $k \in \mathbb{Z}$. □

Finally, to apply Hopf bifurcation theory, we need the following simple-root condition and a computable condition which yields transversality. For simplicity, we denote $r_*^{(k)} := r_*^{(k)}(w_*)$.

Condition (C1): $Q'(w_*) \neq 0$, and all other positive solutions to $Q(\cdot) = 0$ are not integer multiples of w_*.
Condition (C2):

$$\frac{\partial}{\partial\lambda}(e^{\lambda r}\cdot\triangle(\lambda, r, s))|_{\lambda=iw_*, r=r_*^{(k)}} \neq 0 \text{ and } \mathrm{Re}(\lambda'(r_*^{(k)})) \neq 0.$$

We thus obtain the following oscillation theorem for two non-identical cells.

Theorem 2.7. *For a fixed* $s \geq 0$, *assume that there exists a positive solution* w_* *to* $Q(\cdot) = 0$ *satisfying* (2.25) *and conditions (C1) and (C2) for some* $r_*^{(k)} > 0$ *and* $k \in \mathbb{Z}$. *Then Hopf bifurcation occurs at* $r = r_*^{(k)}$ *and an asynchronous periodic orbit is bifurcated from* $\mathbb{X}^*$ *in system* (2.18).

In what follows, we provide an example to show that if system (2.18) of two non-identical cells satisfies the conditions in Theorem 2.7, then the amplitudes of the bifurcated asynchronous periodic solution for the two cells are distinct.

Example 2.2. For system (2.18), we set

$$\begin{aligned} &a_2 = a_4 = 4.5,\ k_H = k_D = 33,\ P_0 = 40,\ P_{D_0} = 400, \\ &\tau_2 = 2.8,\ \tau_3 = 40,\ \tau_4 = 20, \end{aligned} \tag{2.27}$$

and choose

$$d_{1(1)} = d_{2(1)} = d_{3(1)} = d_{4(1)} = 1,\ d_{1(2)} = d_{2(2)} = d_{3(2)} = d_{4(2)} = 1.2. \tag{2.28}$$

Then the system satisfies the conditions in Theorem 2.7 and admits a bifurcated asynchronous periodic solution when τ_1 is near $r_c - \tau_2 \approx 4.13373 - 2.8 = 1.33373$.

In Fig. 1, the periods of the oscillation for cell 1 and cell 2 are the same, but the amplitude of the oscillation for cell 1 is larger than the one of cell 2. We interpret that admitting smaller amplitude for cell 2 corresponds to the degradation rates closer to the values where the oscillations arrest.

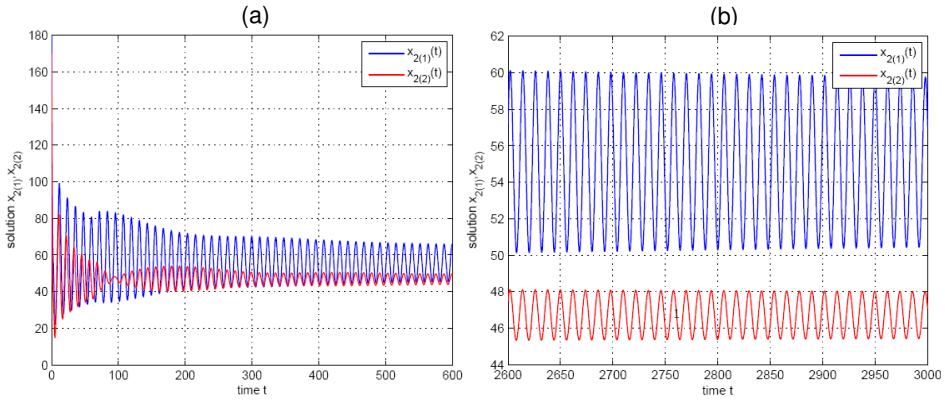

FIGURE 1. Time series of $x_{2(1)}(t)$ and $x_{2(2)}(t)$ in system (2.18) with parameters (2.27) and degradation rates (2.28), from initial value $\phi = (10,\ 180,\ 7,\ 130,\ 8,\ 170,\ 6,\ 138)$, for (a) $t \in [0, 600]$, (b) $t \in [2600, 3000]$. The period of the solution is close to 12 minutes, but the amplitudes of $x_{2(1)}(t)$ and $x_{2(2)}(t)$ are about 9.34 and 2.57, respectively.

Remark 2.3. (i) Theorem 2.7 implicates that two coupled cells with different degradation rates exhibit asynchronous oscillations under certain conditions. Hence, the considered model (2.1) has the potential to generate moving oscillatory wave in a lattice system, if the cells located in the TWR possess pertinent gradient of the degradation rates along the AP axis. (ii) If the solutions w_* to $Q(\cdot) = 0$ satisfy (2.25), then the stability of the bifurcated asynchronous periodic solution can be analyzed by the center manifold theorem and the normal form method, as performed in [19] for the system of two identical cells.

2.3. **Collective behaviors.** So far, we have studied global convergence of dynamics for the n-cell lattice model (2.1), synchronous oscillations over identical cells, and asynchronous oscillation for non-identical cells. In this subsection, we summarize these dynamics and connect them to the corresponding biological scenarios, depicted in Fig. 2.

(D1): Identical cells located at the TB exhibit synchronous oscillations. This dynamics can be examined via Hopf bifurcation theory for the system (2.5) of n identical cells. The parameter and delay conditions for such dynamics are as the ones for the system of two identical cells.

(D2): Cells located at the TWR with different degradation rates admit asynchronous oscillations. Moreover, if we consider two coupled non-identical cells, then this asynchronous oscillation can be examined via Theorem 2.7.

(D3): The oscillatory gene expressions arrest and tend to high and low expression levels for non-identical cells with large degradation rates, located at the DR. This dynamics is obtained in Theorem 2.5 for general coupled n-cell system (2.1).

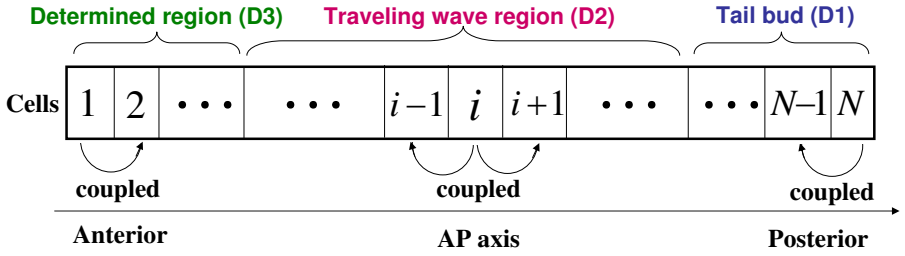

FIGURE 2. N cells aligned in the AP axis, each cell is coupled with its nearest neighbors. The PSM which contains the traveling wave region and the tail bud moves posteriorly as the embryo grows.

Based on these theoretical results, in section 3, we construct a non-autonomous lattice system with gradients of degradation rates and delays to exhibit the biological scenarios in the TB, TWR, and DR.

3. **Traveling wave in non-autonomous system.** It has been observed in biological experiments that normal segmentation requires a pertinent traveling wave of gene expressions propagating from the posterior toward the anterior of the TWR, with increasing period, decreasing amplitude, wave length, and wave speed. Herein, the wave speed is referred to the speed of peaks in the oscillations.

In this section, we shall explore the traveling wave patterns in the N-cell model equations. Based on the theoretical results and the understanding on the dynamics of the two-cell system in [19] and the n-cell system (2.1) established in section 2, we shall design suitable gradients of degradation rates and delay magnitudes to produce traveling wave patterns. This will lead to a non-autonomous lattice system where some degradation rates and delay magnitudes vary with respect to space and time. More precisely, we take into account the dynamics regimes in (D1) to generate synchronous oscillations in the TB, in (D3) to arrest the oscillations in the DR, and combine the dynamics in (D2) and the cell-cell system to devise the gradients of degradation rates and delays. Under suitable design on the gradients, this lattice system can generate various traveling wave patterns, but only some of them represent normal segmentation. As one of the main issues in current investigations of somitogenesis is to explore the cause of mutant, we shall pursue the factors that result in inappropriate propagation of waves, including wrong direction of waves and collision of oscillations and peaks.

We assume that there are N cells located along the AP axis, which are divided into three parts: DR, TWR, and TB, successively, and the PSM contains the TB and TWR. The gene expressions for cells at the TB show synchronous oscillations with period about 30 minutes; the oscillations then slow down with increasing period in the TWR, where traveling wave of gene expression proceeds from the posterior to the anterior. Finally, the oscillations arrest and cells develop into somites in the DR.

According to the experiments, during the growth of the embryo, the cells located at the anterior end of the TWR are removed from the TWR and become mature somites. Meanwhile, the cells located behind the posterior end of the TWR enter the TWR to compensate the loss of anterior cells. Moreover, the growth rate of the embryo is close to a constant. Therefore, this scenario indicates that the overall

length of the TWR maintains a constant value and the PSM moves posteriorly with a constant speed, along with the growth of embryo. According to these observations, we assume that the length of the TWR is constant, denoted by L, and the PSM moves posteriorly with a constant speed $v := 1/m$ which matches the growth rate of the embryo, where L is an integer and m is a positive real number. When $t = 0$, the DR lies in $0 \le i \le K-1$, the TWR is in $K \le i \le K+L-1$, and the TB is in $i \ge K+L$, where K is an integer. Furthermore, for each t with $m(\tilde{k}-1) < t \le m\tilde{k}$, the DR lies in $i \le K+\tilde{k}-2$, and the TWR is in $K+(\tilde{k}-1) \le i \le (K+L-1)+(\tilde{k}-1)$ with the anterior and posterior ends of the TWR at $K+(\tilde{k}-1)$ and at $(K+L-1)+(\tilde{k}-1)$ respectively; the TB is in $i \ge K+L+(\tilde{k}-1)$. Fig. 3 displays the regions TB, TWR, and DR along the AP axis, for $\tilde{k} \in \mathbb{N}$. In addition, the dynamics in regions TB, TWR, and DR correspond to (D1), (D2), and (D3) regimes, depicted in section 2.3, respectively.

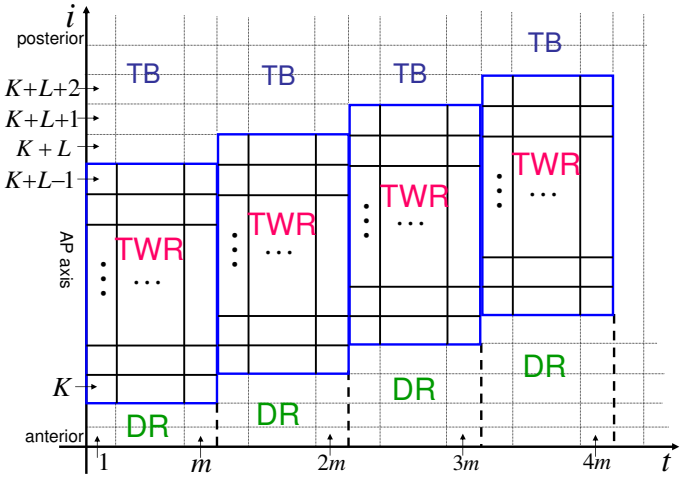

FIGURE 3. The region anterior (resp., posterior) to the TWR is the DR (resp., the TB). The blue blocks represent the TWR which moves posteriorly one grid per m minutes as the embryo grows with speed $v = 1/m$.

To generate oscillatory traveling waves, we propose the following non-autonomous lattice system modified from (2.1):

$$\begin{cases} \dot{x}_{1(i)}(t) &= g_H(x_{2(i)}(t-\tau_{1(i)}(t)),\ \tilde{x}_{4(i)}(t-\tau_{1(i)}(t))) - d_{(i)}(t)x_{1(i)}(t) \\ \dot{x}_{2(i)}(t) &= a_2 x_{1(i)}(t-\tau_2) - d_{(i)}(t)x_{2(i)}(t) \\ \dot{x}_{3(i)}(t) &= g_D(x_{2(i)}(t-\tau_3)) - d_{(i)}(t)x_{3(i)}(t) \\ \dot{x}_{4(i)}(t) &= a_4 x_{3(i)}(t-\tau_4) - d_{(i)}(t)x_{4(i)}(t), \end{cases} \tag{3.1}$$

for $1 \le i \le N$, where g_H and g_D are defined as (2.2) and (2.3) respectively, and the parameters and delays are adopted from Lewis [11, 18, 23]:

$$a_2 = a_4 = 4.5,\ k_D = k_H = 33,\ P_0 = 40,\ P_{D_0} = 400,\ \tau_2 = 2.8,\ \tau_4 = 20, \tag{3.2}$$

$$\tau_1 = 3.8 \pm 1.0 + T_{\text{init}-\text{her}},\ \tau_3 = 8.4 \pm 1.2 + T_{\text{init}-\text{delta}}, \tag{3.3}$$

where $T_{\text{init}-\text{her}}$ (resp., $T_{\text{init}-\text{delta}}$) is the time for bound inhibitory protein and for the mRNA polymerase to produce sufficient transcription for *her1* (resp., *delta*)

gene. Note that the degradation rates

$$d_1 = 0.252525,\ d_2 = 0.23,\ d_3 = 0.273224,\ d_4 = 0.23,$$

adopted in a two-cell system in [23] for the wild type, are close to each other. Therefore, for simplicity, we set all degradation rates of a single cell identical at any time (but different cells can have different degradation rates) in system (3.1). This will allow us to focus on the effect from the gradient of degradation rates with respect to space (i).

From the numerical simulation on system (3.1), if we set the same constant degradation rates for all cells ($d_{(i)} = d$ for all i) and let $\tau_{1(i)}$ decrease (resp., increase) as i decreases, then the system generates oscillatory wave from the anterior (resp., posterior) to the posterior (resp., anterior) of the TWR. Hence, the delay magnitudes play an important role in the direction of wave propagation. On the other hand, the molecular gradients, such as FGF and Wnt signaling, control the period of oscillation for individual cell and cause oscillation-arrested. Hence, similar to the formulation in [30], we set the degradation rates to vary as a reaction to these molecular gradients, during the process. By combining these two factors, we shall design the non-autonomous system (3.1) with degradation and delay gradients to generate various oscillatory wave patterns.

Let us first classify the degradation rates. We denote $d_* = d_j = d_{j(i)}$, $j = 1, 2, 3, 4$, $i = 1, 2$, in the system of two identical cells. According to our analysis (Corollary 3.7 and Fig. 3 of [19]), with the parameters in (3.2), if we fix $s = \tau_3 + \tau_4$, then the ranges for d_* to have stable synchronous periodic solution and to have stable asynchronous periodic solution appear in successive subintervals, one next to the other. We denote these subintervals as I_S, I_{AS}, and I_{SS}, where $I_S \cup I_{SS}$ (resp., I_{AS}) contains the degradation rates d_* with which the system admits a stable synchronous (resp., asynchronous) periodic solution when $d_{j(i)} = d_j = d_*$, $j = 1, 2, 3, 4$, $i = 1, 2$, and r near the minimal bifurcation value r_c, via Hopf bifurcation. Moreover, from Hopf bifurcation theory, only synchronous periodic solutions appear when $d_* \in I_{SS}$, and either synchronous or asynchronous oscillation can occur when $d_* \in I_S$. In addition, the interval I_{SS} is usually located on the right of $I_S \cup I_{AS}$. For example, when $s = 60$ ($\tau_3 = 40$, $\tau_4 = 20$),

$$I_S \cup I_{AS} = [0.15,\ 1.3865] \text{ and } I_{SS} = [s_a,\ s_b] := [1.38652,\ 1.38824]. \tag{3.4}$$

Next, we employ the function $p_s := p_s(d_*)$ to delineate the periods of these oscillations, for a given $s \geq 0$. In Fig. 4, for $s = 60$, we depict $p_s(d_*)$ for $d_* \in S_d := \{0.15,\ 0.16, \cdots, 1.37,\ 1.38,\ 1.3865\}$. It is interesting to see that the period $p_s(d_*)$ decreases (resp., increases) with respect to $d_* \in \{0.15,\ 0.16, \cdots,\ 0.94,\ 0.95\}$, (resp., $\{0.96,\ 0.97, \cdots,\ 1.37,\ 1.38,\ 1.3865\}$). Based on this variation of period in Fig. 4, for convenience, we set

$$I_{\text{pd}} := [0.15,\ 0.95] \text{ and } I_{\text{pi}} := [0.96,\ 1.3865]. \tag{3.5}$$

We specify two degradation rates, d_c and d_s, for the setting of degradation gradient in (3.1). Let d_c be a quantity satisfying condition (2.16), so that there is a globally asymptotically stable synchronous equilibrium $\bar{\mathbb{X}}$ for system (2.5) with $d_j = d_c$, $j = 1, 2, 3, 4$, for any fixed $r = \tau_1 + \tau_2 \geq 0$ and $s = \tau_3 + \tau_4 \geq 0$. On the other hand, with $d_j = d_s$, $j = 1, 2, 3, 4$, there exists a stable periodic solution bifurcated at r_c via Hopf bifurcation theory. Furthermore, we can find the *her* transcription delay, τ_s, such that $\tau_s + \tau_2$ is the minimal bifurcation value r_c for the system with parameters

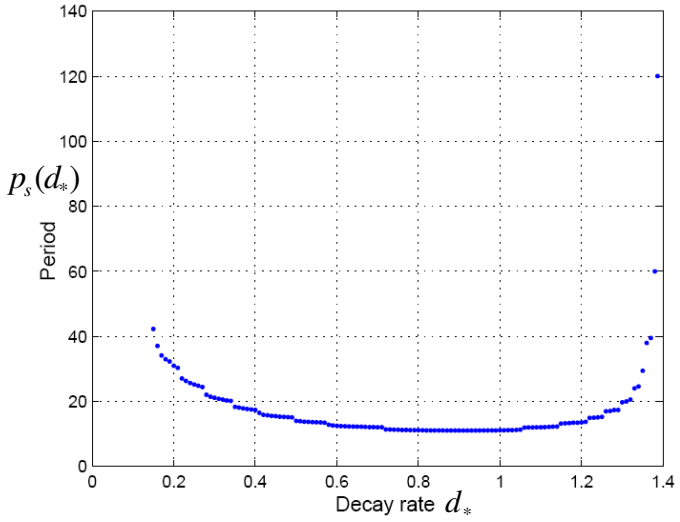

FIGURE 4. The periods of oscillations, $p_s(d_*)$, corresponding to a sequence of $d_* \in S_d$, in the system of two identical cells with degradation rates $d_{j(i)} = d_j = d_*$, $j = 1, 2, 3, 4$, $i = 1, 2$, when $r = \tau_1 + \tau_2$ is close to the minimal bifurcation value r_c.

(3.2) and degradation rate d_s. Accordingly, we choose $d_s \in I_S \cup I_{SS}$ to generate oscillations, and take $d_c > d_s$ as larger degradation rates to create oscillation-arrested. Next, we choose some value $d_\ell \in (d_s,\ d_c)$ so that the system with parameters (3.2) and degradation rate d_ℓ has a stable periodic solution bifurcated at the minimal bifurcation value $r_c = \tau_\ell + \tau_2$.

We set the degradation rates equal to d_c and d_s, for the cells at the DR and TB respectively, so that oscillation-arrested in the DR and synchronous oscillation with period $p_s(d_s)$ in the TB take place, according to regimes (D3) and (D1) respectively. Moreover, we let the degradation rates vary from d_s at the posterior end to d_ℓ at the anterior end of the TWR. In addition, we divide the TWR into three parts $R_3,\ R_2$, and R_1, from the anterior to the posterior, so that the degradation rates are continuous and decreasing linearly, delay $\tau_{1(i)}$ is continuous and linear in each region, and the absolute values of the slope of degradation rate and $\tau_{1(i)}$ are largest (resp., smallest) in R_3 (resp., R_1). The arrangement is according to the dependence of the gradient slopes in $d_{(i)}$ and $\tau_{1(i)}$ on the rate of period variation of the oscillations. Based on this setting, we design $d_{(i)}(t)$ and $\tau_{1(i)}(t)$ for system (3.1) in the following five regions. We denote $\tilde{d} = (d_\ell - d_s)/3$ and $\tilde{\tau} = (\tau_\ell - \tau_s)/3$, and set $d_{(i)}(t)$ and $\tau_{1(i)}(t)$ for cell i at time t in the respective region as follows:
(i) $1 \le i \le K - 1$, i.e., the determined region initially,

$$\begin{aligned} d_{(i)}(t) &= d_c, \text{ for } t \ge 0, \\ \tau_{1(i)}(t) &= \tau_\ell, \text{ for } t \ge 0; \end{aligned}$$

(ii) $K \le i \le K + L/6 - 1$, i.e., region R_3 initially,

$$d_{(i)}(t) = \begin{cases} d_{0(i)} + t\frac{d_\ell - d_{0(i)}}{m(i-K+1)}, \text{ for } 0 \le t \le m(i-K+1), \\ d_c, \text{ for } t > m(i-K+1), \end{cases}$$

$$\tau_{1(i)}(t) = \begin{cases} \tau_{0(i)} + t\frac{\tau_\ell - \tau_{0(i)}}{m(i-K+1)}, \text{ for } 0 \le t \le m(i-K+1), \\ \tau_\ell, \text{ for } t > m(i-K+1), \end{cases}$$

where $d_{0(i)} = d_\ell - \frac{6\tilde{d}}{L}(i-K+1)$ and $\tau_{0(i)} = \tau_\ell - \frac{6\tilde{\tau}}{L}(i-K+1)$;
(iii) $K + L/6 \le i \le K + L/2 - 1$, i.e., region R_2 initially,

$$d_{(i)}(t) = \begin{cases} d_{0(i)} + t\frac{(d_\ell - \tilde{d}) - d_{0(i)}}{m(i-K-L/6+1)}, \text{ for } 0 \le t \le m(i-K-L/6+1), \\ (d_\ell - \tilde{d}) + (t - m(i-K-L/6+1))\frac{6\tilde{d}}{mL}, \\ \qquad\qquad \text{for } m(i-K-L/6+1) < t \le m(i-K+1), \\ d_c, \text{ for } t > m(i-K+1), \end{cases}$$

$$\tau_{1(i)}(t) = \begin{cases} \tau_{0(i)} + t\frac{(\tau_\ell - \tilde{\tau}) - \tau_{0(i)}}{m(i-K-L/6+1)}, \text{ for } 0 \le t \le m(i-K-L/6+1), \\ (\tau_\ell - \tilde{\tau}) + (t - m(i-K-L/6+1))\frac{6\tilde{\tau}}{mL}, \\ \qquad\qquad \text{for } m(i-K-L/6+1) < t \le m(i-K+1), \\ \tau_\ell, \text{ for } t > m(i-K+1), \end{cases}$$

where $d_{0(i)} = (d_\ell - \tilde{d}) - \frac{3\tilde{d}}{L}(i-K-L/6+1)$ and $\tau_{0(i)} = (\tau_\ell - \tilde{\tau}) - \frac{3\tilde{\tau}}{L}(i-K-L/6+1)$;
(iv) $K + L/2 \le i \le K + L - 1$, i.e., region R_1 initially,

$$d_{(i)}(t) = \begin{cases} d_{0(i)} + t\frac{(d_\ell - 2\tilde{d}) - d_{0(i)}}{m(i-K-L/2+1)}, \text{ for } 0 \le t \le m(i-K-L/2+1), \\ (d_\ell - 2\tilde{d}) + (t - m(i-K-L/2+1))\frac{3\tilde{d}}{mL}, \\ \qquad\qquad \text{for } m(i-K-L/2+1) < t \le m(i-K-L/6+1), \\ (d_\ell - \tilde{d}) + (t - m(i-K-L/6+1))\frac{6\tilde{d}}{mL}, \\ \qquad\qquad \text{for } m(i-K-L/6+1) < t \le m(i-K+1), \\ d_c, \text{ for } t > m(i-K+1), \end{cases}$$

$$\tau_{1(i)}(t) = \begin{cases} \tau_{0(i)} + t\frac{(\tau_\ell - 2\tilde{\tau}) - \tau_{0(i)}}{m(i-K-L/2+1)}, \text{ for } 0 \le t \le m(i-K-L/2+1), \\ (\tau_\ell - 2\tilde{\tau}) + (t - m(i-K-L/2+1))\frac{3\tilde{\tau}}{mL}, \\ \qquad\qquad \text{for } m(i-K-L/2+1) < t \le m(i-K-L/6+1), \\ (\tau_\ell - \tilde{\tau}) + (t - m(i-K-L/6+1))\frac{6\tilde{\tau}}{mL}, \\ \qquad\qquad \text{for } m(i-K-L/6+1) < t \le m(i-K+1), \\ \tau_\ell, \text{ for } t > m(i-K+1), \end{cases}$$

where $d_{0(i)} = (d_\ell - 2\tilde{d}) - \frac{2\tilde{d}}{L}(i-K-L/2+1)$ and $\tau_{0(i)} = (\tau_\ell - 2\tilde{\tau}) - \frac{2\tilde{\tau}}{L}(i-K-L/2+1)$;
(v) $K + L \le i \le N$, i.e., the tail bud initially,

$$d_{(i)}(t) = \begin{cases} d_s, \text{ for } 0 \le t \le m(i-K-L+1), \\ d_s + (t - m(i-K-L+1))\frac{2\tilde{d}}{mL}, \\ \qquad\qquad \text{for } m(i-K-L+1) < t \le m(i-K-L/2+1), \\ (d_\ell - 2\tilde{d}) + (t - m(i-K-L/2+1))\frac{3\tilde{d}}{mL}, \\ \qquad\qquad \text{for } m(i-K-L/2+1) < t \le m(i-K-L/6+1), \\ (d_\ell - \tilde{d}) + (t - m(i-K-L/6+1))\frac{6\tilde{d}}{mL}, \\ \qquad\qquad \text{for } m(i-K-L/6+1) < t \le m(i-K+1), \\ d_c, \text{ for } t > m(i-K+1), \end{cases}$$

$$\tau_{1(i)}(t) = \begin{cases} \tau_s, \text{ for } 0 \le t \le m(i-K-L+1), \\ \tau_s + (t - m(i-K-L+1))\frac{2\tilde{\tau}}{mL}, \\ \qquad \text{for } m(i-K-L+1) < t \le m(i-K-L/2+1), \\ (\tau_\ell - 2\tilde{\tau}) + (t - m(i-K-L/2+1))\frac{3\tilde{\tau}}{mL}, \\ \qquad \text{for } m(i-K-L/2+1) < t \le m(i-K-L/6+1), \\ (\tau_\ell - \tilde{\tau}) + (t - m(i-K-L/6+1))\frac{6\tilde{\tau}}{mL}, \\ \qquad \text{for } m(i-K-L/6+1) < t \le m(i-K+1), \\ \tau_\ell, \text{ for } t > m(i-K+1). \end{cases}$$

Figs. 5, 6 depict the degradation rate $d_{(i)}(t)$ and delay magnitude $\tau_{1(i)}(t)$ with respect to space (i) respectively; the considered spatiotemporal domain is also illustrated in Fig. 5. Since the traveling wave region moves posteriorly as time evolves, the degradation rate $d_{(i)}(t)$ and delay $\tau_{1(i)}(t)$ vary with time, for each i.

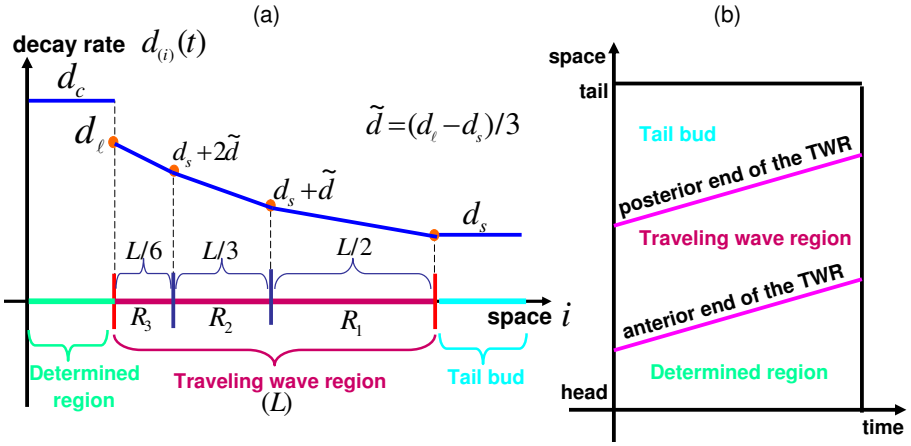

FIGURE 5. Diagrams for (a) the gradient of degradation rate $d_{(i)}(t)$ with respect to space, and (b) the spatiotemporal domain.

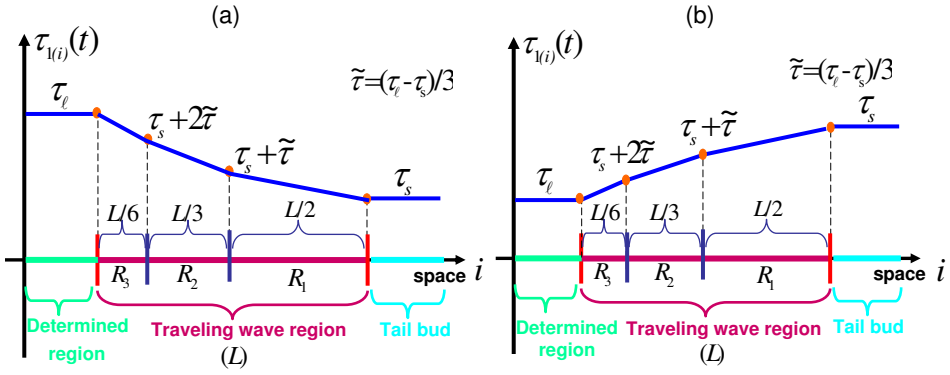

FIGURE 6. Diagrams for the gradient of $\tau_{1(i)}(t)$ when (a) $\tau_\ell > \tau_s$ and (b) $\tau_\ell < \tau_s$.

Notice that, if we take $d_{(i)}(t) = d_c = 2.3$ for each i and all t, in the N-cell system (3.1), then $\bar{\mathbb{X}} = (\bar{\mathbf{x}}, \cdots, \bar{\mathbf{x}})$ is a globally asymptotically stable synchronous

equilibrium for (3.1), where

$$\bar{\mathbf{x}} \approx (11.1778,\ 21.8696,\ 11.0459,\ 21.6116).$$

For explicit illustration, we take $d_c = 2.3$ and the constant initial values for the cells at the DR as

$$x_{1(i)}(s) = 11.1778,\ x_{2(i)}(s) = 21.8696,\ x_{3(i)}(s) = 11.0459,\ x_{4(i)}(s) = 21.6116, \tag{3.6}$$

for $s \in [-\tau_M, 0]$, and $1 \le i \le K-1$. Next, for the cells at the TWR and TB, we take the constant initial values decreasing linearly from the values in (3.6) to zero. That is,

$$x_{1(i)}(s) = 11.1778(1 - \tfrac{i-K+1}{N-K+1}), \quad x_{2(i)}(s) = 21.8696(1 - \frac{i-K+1}{N-K+1}),$$
$$x_{3(i)}(s) = 11.0459(1 - \tfrac{i-K+1}{N-K+1}), \quad x_{4(i)}(s) = 21.6116(1 - \frac{i-K+1}{N-K+1}),$$

for $s \in [-\tau_M, 0]$, and $K \le i \le N$.

Under the gradient setting, our numerical simulations show that traveling wave formation for system (3.1) strongly depends on how we choose d_c, d_s, and d_ℓ, and the subsequent delay magnitudes. Through these simulations, we also hope to observe the clue for the regimes of normal and abnormal segmentation from period variation $p_s(d_*)$ in Fig. 4. We summarize the traveling wave patterns with respect to subinterval $[d_s,\ d_\ell]$ chosen in the simulations, in the following (I). We then illustrate the normal traveling wave patterns in (II). We only present the cases for $s = 60$ ($\tau_3 = 40$, $\tau_4 = 20$), since the patterns are similar to other value of s, and we only demonstrate the contours for component $x_{2(i)}(t)$, $i = 1, \cdots, N$, of system (3.1) with $N = 150$, $K = 11$, $L = 60$, $m = 10$. Recall that $I_{\rm pd}$ and $I_{\rm pi}$ were introduced in (3.5).

(I) Classification of traveling wave patterns:
(i) If $[d_s,\ d_\ell] \subseteq I_{\rm pd}$, then system (3.1) generates a traveling wave pattern emerging from the anterior end of the TWR and moving toward the posterior with separated peaks, as shown in Fig. 7. Moreover, the periods and amplitudes decrease as the wave approaches the anterior of the TWR. This wave corresponds to incorrect propagation of signals.
(ii) If $[d_s,\ d_\ell] \subseteq I_{\rm pi}$, then system (3.1) generates a traveling wave pattern emerging from the posterior end of the TWR and moving toward the anterior with separated peaks, as illustrated in Fig. 8. Moreover, the period increases, and the amplitude, wave length, and wave speed become smaller as the wave approaches the anterior of the TWR.
(iii) If $d_s \in I_{\rm pd}$ and $d_\ell \in I_{\rm pi}$, then there are some possibilities, depending on the value of d_ℓ. Basically, if d_ℓ is not large enough, then the peaks of the oscillatory wave propagate in wrong direction. However, the direction could be modified and reversed by increasing d_ℓ.

In Figs. 9(a), 9(b), and 9(c), we consider system (3.1) with $d_s = 0.17$, and $d_\ell = 1.35, 1.38$, and 1.3865 respectively. In Fig. 9(a), the wave moves posteriorly. In Fig. 9(b), the slopes of the contours vary from positive to negative as the peaks approach the anterior end of the TWR; in Fig. 9(c), the slopes are negative, i.e., the wave moves anteriorly. That is, the slopes of the contour decrease from positive to negative as d_ℓ increases. Therefore, the wave emerges from the posterior and moves anteriorly, i.e., in right direction, if d_ℓ is large.

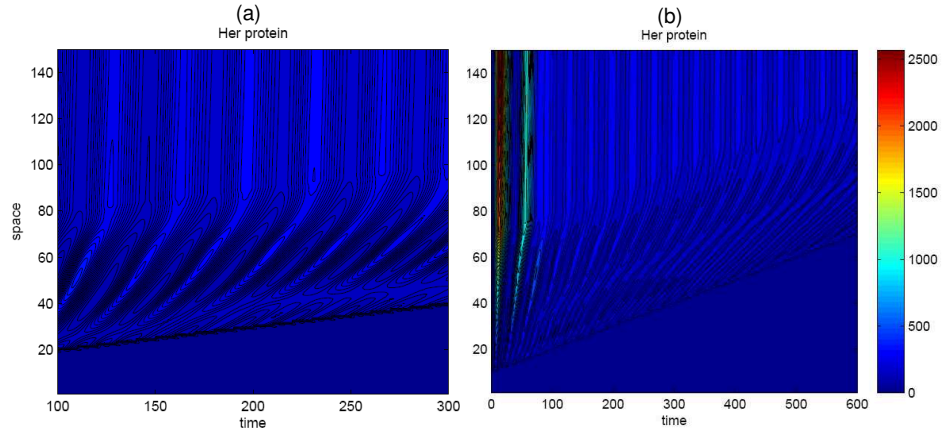

FIGURE 7. Traveling wave patterns for system (3.1) with (a) $[d_s,\ d_\ell] = [0.17,\ 0.34] \subseteq I_{\text{pd}}$ and $[\tau_s,\ \tau_\ell] = [5.34241,\ 2.18761]$, $p_s(d_s) \approx 34.0909$ and $p_s(d_\ell) \approx 20.1342$, (b) $[d_s,\ d_\ell] = [0.17,\ 0.48] \subseteq I_{\text{pd}}$ with $[\tau_s,\ \tau_\ell] = [5.34241,\ 1.15009]$, $p_s(d_s) \approx 34.0909$ and $p_s(d_\ell) \approx 15.1515$. The waves emerge from the anterior end of TWR and move toward the posterior of TWR with increasing period.

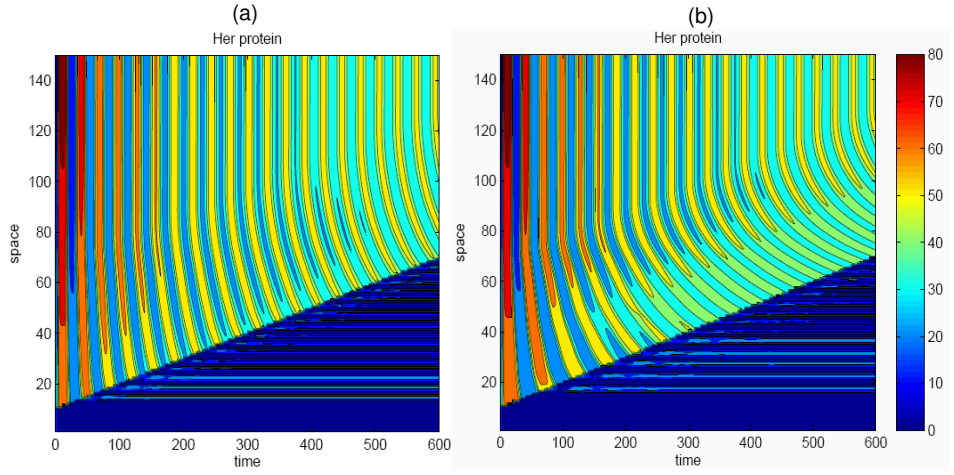

FIGURE 8. The solutions of system (3.1) for $d_s = 1.34238$, and $\tau_s = 10.1358$ with $p_s(d_s) \approx 29.129$, and (a) $d_\ell = 1.36$ and $\tau_\ell = 14.7993$ with $p_s(d_\ell) \approx 37.9795$, (b) $d_\ell = 1.38$ and $\tau_\ell = 25.5646$ with $p_s(d_\ell) \approx 59.988$. All these correspond to normal gene expression patterns in the TB, TWR, and DR.

Another type of defect is depicted in Fig. 10 where the peaks not only move in inappropriate direction, but also collide. Similarly, by increasing the value of d_ℓ, the peaks can become separated and the direction of the wave be modified, see Fig. 10(b).

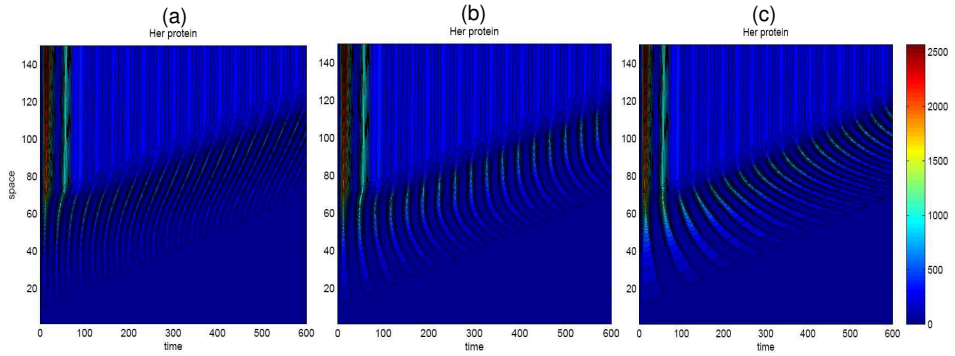

FIGURE 9. The solutions of system (3.1) for $d_s = 0.17$, and $\tau_s = 5.34241$ with $p_s(d_s) \approx 34.0909$, and (a) $d_\ell = 1.35$, $\tau_\ell = 10.4041$ with $p_s(d_\ell) \approx 29.4118$, (b) $d_\ell = 1.38$, $\tau_\ell = 25.5646$ with $p_s(d_\ell) \approx 59.988$, (c) $d_\ell = 1.3865$ and $\tau_\ell = 57.2218$ with $p_s(d_\ell) \approx 120.005$. The slopes for the contours of the peaks decrease from positive to negative as d_ℓ increases.

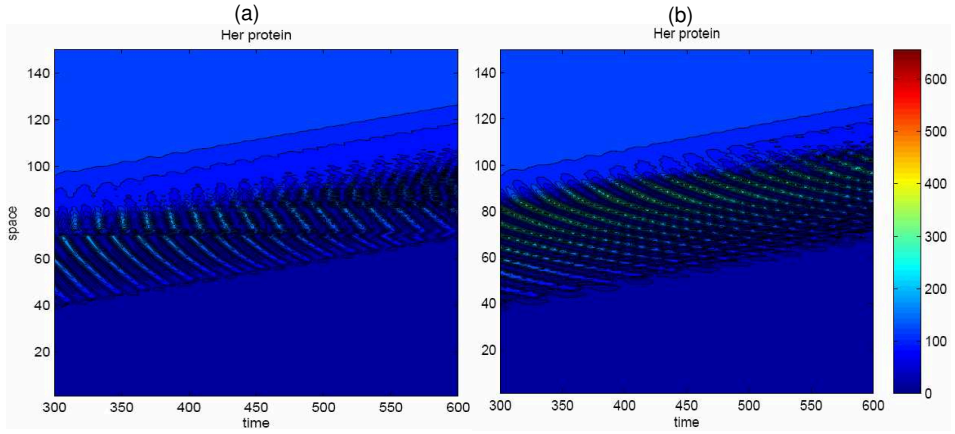

FIGURE 10. The solutions of system (3.1) for $d_s = 0.37$, and $\tau_s = 1.63856$ with $p_s(d_s) \approx 17.8571$ and (a) $d_\ell = 1.33$, $\tau_\ell = 7.50682$ with $p_s(d_\ell) \approx 23.9981$, (b) $d_\ell = 1.38$, $\tau_\ell = 25.5646$ with $p_s(d_\ell) \approx 59.988$. The peaks collide in (a) and become separated as d_ℓ increases from 1.33 in (a) to 1.38 in (b). Herein, although $d_s = 0.37 \in I_{AS}$, the system still generates synchronous oscillation in the TB.

Therefore, Figs. 9 and 10 demonstrate that large d_ℓ could modify the direction of the traveling wave pattern. We interpret this as that the system tends to produce traveling wave with proper moving direction, if the degradation rates of the cells located at the anterior end of the TWR are large enough. In addition, we also observe that if $d_s \in I_{\text{pd}}$ and $d_\ell \in I_{\text{pi}}$, then the variation of amplitude is either abrupt or out of accord with position in regions TB and TWR, no matter how d_ℓ is enlarged.

(iv) (a) If $d_\ell \approx s_a$, the left end point of interval I_{SS}, then the generated wave almost stops in the TWR. (b) If $(d_\ell - s_a)$ is large enough, then the generated wave moves toward the posterior of the TWR. Both of these two cases correspond to abnormal patterns.

(II) Normal traveling wave pattern:
According to the classification in (I), the case (ii): $[d_s, d_\ell] \subseteq I_{\rm pi}$ is the regime for traveling wave pattern with normal direction and amplitude. Let us demonstrate such patterns by setting $d_s = 1.34238 \in I_{\rm pi}$ with period $p_s(1.34238) \approx 29.129$ minutes to generate synchronous oscillation in the TB. In addition, for any given d_ℓ with $d_\ell > d_s$, the lattice system (3.1) produces traveling wave which propagates in pertinent rhythm and direction in the TWR. Moreover, the wave length becomes narrower and the absolute value of wave speed becomes smaller as the wave moves toward the anterior of the TWR.

Next, in order to generate high and low expression levels in the DR, we choose two degradation rates $d_{c\ell}$ and d_{cs} with $d_{c\ell} > d_{cs}$. If the peak (resp., foot) of oscillation arrives the anterior end of the TWR at cell $i_{\rm p}$ (resp., $i_{\rm f}$) and time $t_{\rm p}$ (resp., $t_{\rm f}$), then we replace the setting in the DR by $d_{(i)}(t) = d_{cs}$, for $i = i_{\rm p}$ and $t \geq t_{\rm p}$ (resp., $d_{(i)}(t) = d_{c\ell}$, for $i = i_{\rm f}$ and $t \geq t_{\rm f}$). Under this setting, the cell $i_{\rm p}$ (resp., $i_{\rm f}$) with smaller (resp., larger) degradation rate d_{cs} (resp., $d_{c\ell}$) admits higher (resp., lower) level of expression in the DR. We set $d_{cs} = 2.3$, $d_{c\ell} = 4$, $d_s = 1.34238$, and d_ℓ equal to 1.36 and 1.38 in Figs. 8(a) and (b), respectively. Fig. 8 exhibits normal oscillatory traveling wave patterns; the periods at the anterior end of the TWR are smaller in Fig. 8(a), as $d_\ell = 1.36$, than the ones in Fig. 8(b), as $d_\ell = 1.38$.

Remark 3.1. In Fig. 8, $d_{cs} = 2.3$ and $d_{c\ell} = 4$ actually do not satisfy condition (2.14); the system still converges to a non-uniform steady state and display the high-low expression level. In fact, we can further increase d_{cs} and $d_{c\ell}$ to meet condition (2.14) and obtain analogous scenario as mentioned in Remark 2.2(i). However, the magnitudes of the gene expressions in the DR are too low for clear demonstration. More detailed discussion on the spatiotemporal patterns can be found in [20].

4. **Conclusion.** In this investigation, we have constructed a non-autonomous lattice system to generate clock-wave pattern corresponding to the cyclic gene expression in the segmentation of zebrafish embryo. Such spatiotemporal patterns exhibit synchronous oscillation in the tail bud, oscillatory waves traveling from the posterior to the anterior of the TWR, oscillation slowing down, and period increasing toward the determined region, and finally oscillation-arrested at the determined region. During the process, the oscillation travels due to the gradients of activation parameters (degradation rates herein) and delay magnitudes. Pertinent gradient structure leads to normal segmentation. In mathematical models, generating such spatiotemporal patterns require understanding the parameter and delay magnitudes which correspond to the chief dynamical phases. Numerical simulations will be difficult to proceed without sufficient information on the dynamics of the systems. Through establishing analytical theories on synchronous oscillations and oscillation-arrested for the autonomous n-cell model, we formulated suitable gradients of degradation rates and transcription delay of *her* mRNA for this non-autonomous lattice system. To elucidate the mechanism for somitogenesis through mathematical modeling, we have made an attempt to map the factors for normal and abnormal segmentations

in the non-autonomous lattice model to the cell-cell dynamics. From this correspondence, we learned the regime for normal spatiotemporal pattern, which correlates to the robust mechanism of somitogenesis. Although the gradient structure adopted herein is piecewise linear, it captures the chief scenario of the clock and wavefront patterns. We only presented the result for the system with gradients of degradation rates and transcription delay of *her* mRNA, the effects on the dynamics and waves from other parameters and delays can be similarly discussed.

Acknowledgments. The authors are grateful to Dr. Yun-Jin Jiang at NHRI of Taiwan for helpful discussions on somitogenesis experiments. This work is supported, in part, by the National Center of Theoretical Sciences and National Science Council of Taiwan, R.O.C.

REFERENCES

[1] N. J. Armstrong, K. J. Painter and J. A. Sherratt, *A continuum approach to modelling cell-cell adhesion*, J. Theoret. Biol., **243** (2006), 98–113.
[2] N. J. Armstrong, K. J. Painter and J. A. Sherratt, *Adding adhesion to a chemical signaling model for somite formation*, Bulletin Math. Biol., **71** (2009), 1–24.
[3] R. E. Baker and S. Schnell, *How can mathematics help us explore vertebrate segmentation?*, HFSP J., **3** (2009), 1–5.
[4] R. E. Baker, S. Schnell and P. K. Maini, *A mathematical investigation of a clock and wavefornt model for somitogenesis*, J. Math. Biol., **52** (2006), 458–482.
[5] M. Campanelli and T. Gedeon, *Somitogenesis clock-wave initiation requires differential decay and multiple binding sites for clock protein*, PLoS Comput. Biol., **6** (2010), e1000728.
[6] O. Cinquin, *Repressor dimerization in the zebrafish somitogenesis clock*, PLoS Comput. Biol., **3** (2007), 293–303.
[7] J. Cooke and E. C. Zeeman, *A clock and wavefront model for control of the number of repeated structures during animal morphogenesis*, J. Theoret. Biol., **58** (1976), 455–476.
[8] J. Dubrulle, M. J. McGrew and O. Pourquié, *FGF signaling controls somite boundary position and regulates segmentation clock control of spatiotemporal Hox gene activation*, Cell, **106** (2001), 219–232.
[9] J. Dubrulle and O. Pourquié, *From head to tail: links between the segmentation clock and antero-posterior patterning of the embryo*, Curr. Opin. Genet. Dev., **12** (2002), 519–523.
[10] J. Dubrulle and O. Pourquié, *fgf8 mRNA decay establishes a gradient that couples axial elongation to patterning in the vertebrate embryo*, Nature, **427** (2004), 419–422.
[11] F. Giudicelli, E. M. Özbudak, G. J. Wright and J. Lewis, *Setting the tempo in development: an investigation of the zebrafish somite clock mechanism*, PLOS Biol., **5** (2007), e150, 1309–1323.
[12] A. Goldbeter and O. Pourquié, *Modeling the segmentation clock as a network of coupled oscillations in the Notch, Wnt and FGF signaling pathways*, J. Theoret. Biol., **252** (2008), 574–585.
[13] E. Hanneman and M. Westerfield, *Early expression of acetyl-choline-sterase activity in functionally distinct neurons of the zebrafish*, J. Comp. Neurol., **284** (1989), 350–361.
[14] S. A. Holley, *The genetics and embryology of zebrafish metamerism*, Dev. Dyn., **236** (2007), 1422–1449.
[15] K. Horikawa, K. Ishimatsu, E. Yoshimoto, S. Kondo and H. Takeda, *Noise-resistant and synchronized oscillation of the segmentation clock*, Nature, **441** (2006), 719–723.
[16] Y.-J. Jiang, B. L. Aerne, L. Smithers, C. Haddon, D. Ish-Horowicz and J. Lewis, *Notch signaling and the synchronization of the somite segmentation clock*, Nature, **408** (2000), 475–479.
[17] A. Kawamura, S. Koshida, H. Hijikata, T. Sakaguchi, H. Kondoh and S. Takada, *Zebrafish hairy/enhancer of split protein links FGF signaling to cyclic gene expression in the periodic segmentation of somites*, Genes Dev., **19** (2005), 1156–1161.
[18] J. Lewis, *Autoinhibition with transcriptional delay: a simple mechanism for the zebrafish somitogenesis oscillator*, Curr Biol., **13** (2003), 1398–1408.

[19] K.-L. Liao, C.-W. Shih and J.-P. Tseng, *Synchronized oscillations in a mathematical model of segmentation in zebrafish*, Nonlinearity, **25** (2012), 869–904.
[20] K.-L. Liao, "Analysis on Mathematical Models of Somitogenesis in Zebrafish," Ph.D thesis, National Chiao Tung University, Hsinchu, 2012.
[21] A. Mara, J. Schroeder, C. Chalouni and S. A. Holley, *Priming, initiation and synchronization of the segmentation clock by deltaD and deltaC*, Nat. Cell. Biol., **9** (2007), 523–530.
[22] L. G. Morelli, S. Ares, L. Herrgen, C. Schröter, F. Jülicher and A. C. Oates, *Delayed coupling theory of vertebrate segmentation*, HFSP J., **3** (2009), 55–66.
[23] E. M. Özbudak and J. Lewis, *Notch signalling synchronizes the zebrafish segmentation clock but is not needed to create somite boundaries*, PLoS Genet., **4** (2008), e15.
[24] O. Pourquié, *The chick embryo: a leading model in somitogenesis studies*, Mech. Dev., **121** (2004), 1069–1079.
[25] I. H. Riedel-Kruse, C. Müller and A. C. Oates, *Synchrony dynamics during initiation, failure, and rescue of the segmentation clock*, Science, **317** (2007), 1911–1915.
[26] J. A. Sherratt and M. J. Smith, *Periodic travelling waves in cyclic populations: field studies and reaction-diffusion models*, J. R. Soc. Interface, **5** (2008), 483–505.
[27] C.-W. Shih and J.-P. Tseng, *Convergent dynamics for multistable delayed neural networks*, Nonlinearity, **21** (2008), 2361–2389.
[28] C.-W. Shih and J.-P. Tseng, *Global synchronization and asymptotic phases for a ring of identical cells with delayed coupling*, SIAM J. Math. Analy., **43** (2011), 1667–1697.
[29] D. Sieger, B. Ackermann, C. Winkler, D. Tautz and M. Gajewski, *her1 and her13.2 are jointly required for somitic border specification along the entire axis of the fish embryo*, Dev. Biol., **293** (2006), 242–251.
[30] K. Uriu, Y. Morishita and Y. Iwasa, *Traveling wave formation in vertebrate segmentation*, J. Theoret. Biol., **257** (2009), 385–396.
[31] K. Uriu, Y. Morishita and Y. Iwasa, *Synchronized oscillation of the segmentation clock gene in vertebrate development*, J. Math. Biol., **61** (2010), 207–229.
[32] M. B. Wahl, C. Deng, M. Lewandoski and O. Pourquié, *FGF signaling acts upstream of the NOTCH and WNT signaling pathways to control segmentation clock oscillations in mouse somitogenesis*, Dev., **134** (2007), 4033–4041.
[33] D. M. Young, "Iteration Solution of Large Linear Systems," Academic Press, New York-London, 1971.

Received April 2011; revised April 2012.

E-mail address: kangling325@gmail.com
E-mail address: cwshih@math.nctu.edu.tw